AD-A043 325 SCIENCE APPLICATIONS INC BEDFORD MASS F/G 19/4
EJECTA SIZING FOR MIDDLE GUST TEST SERIES AND A REVIEW OF EJECT--ETC(U)
DEC 76 H J LINNERUD DNA001-76-C-0109
UNCLASSIFIED SAI-76-507-BOS DNA-4230F NL

| OF |
AD
A043 325

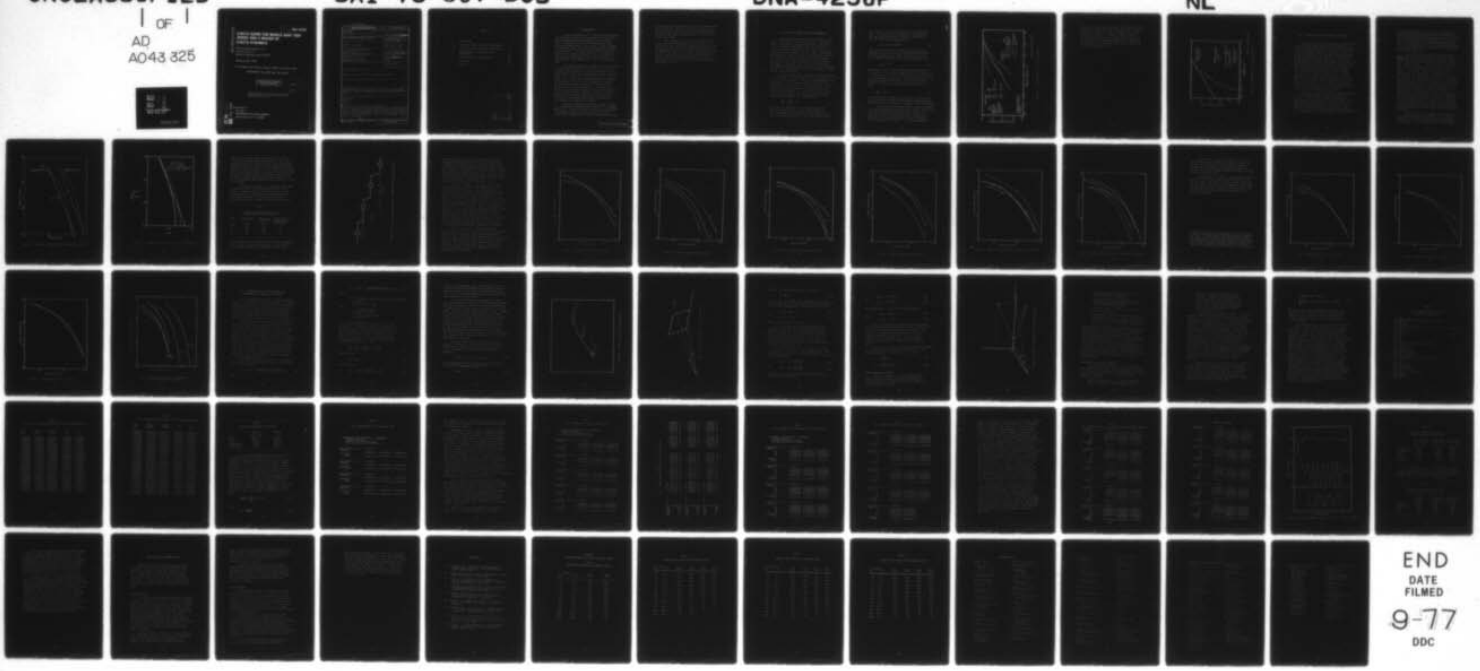

END
DATE FILMED
9-77
DDC

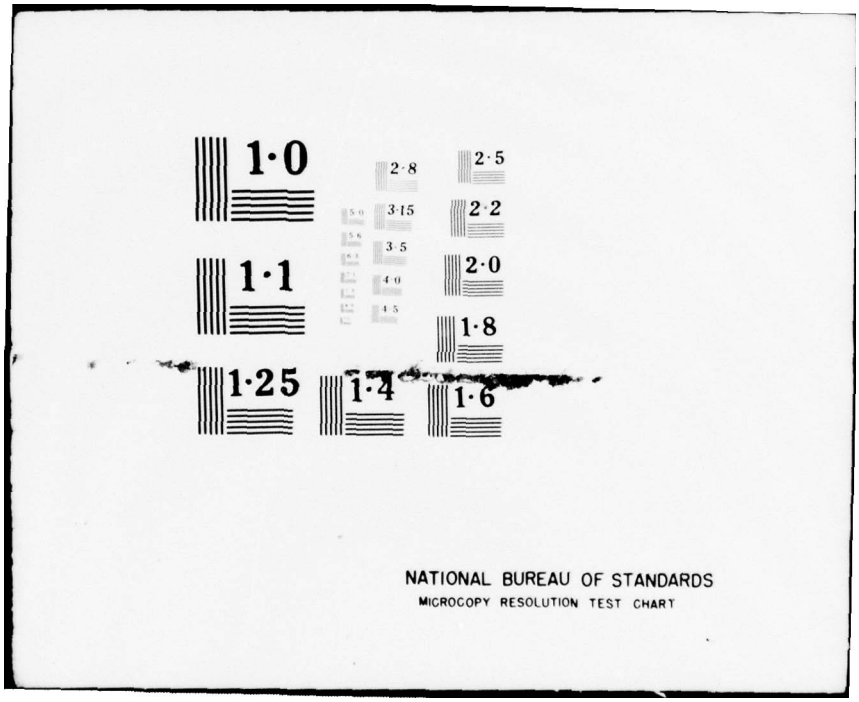
1·0
1·1
1·25
1·4
1·6
1·8
2·0
2·2
2·5
2·8
3·15
3·5
4·0
4·5
5·0
5·6
6·3
NATIONAL BUREAU OF STANDARDS
MICROCOPY RESOLUTION TEST CHART

DNA 4230F

EJECTA SIZING FOR MIDDLE GUST TEST SERIES AND A REVIEW OF EJECTA DYNAMICS

Science Applications, Inc.
3 Preston Court
Bedford, Massachusetts 01730

29 December 1976

Final Report for Period 1 August 1975—1 October 1976

CONTRACT No. DNA 001-76-C-0109

THIS WORK SPONSORED BY THE DEFENSE NUCLEAR AGENCY
UNDER RDT&E RMSS CODES B344076464 Y99QAXSA00178 AND
B34407T464 Y99QAXSC00201 H2590D.

Prepared for
Director
DEFENSE NUCLEAR AGENCY
Washington, D. C. 20305

UNCLASSIFIED

SECURITY CLASSIFICATION OF THIS PAGE *(When Data Entered)*

REPORT DOCUMENTATION PAGE		READ INSTRUCTIONS BEFORE COMPLETING FORM
1. REPORT NUMBER DNA 4230F	2. GOVT ACCESSION NO.	3. RECIPIENT'S CATALOG NUMBER
4. TITLE *(and Subtitle)* EJECTA SIZING FOR MIDDLE GUST TEST SERIES AND A REVIEW OF EJECTA DYNAMICS		5. TYPE OF REPORT & PERIOD COVERED Final Report ~~for Period~~ 1 Aug 75—1 Oct 76 6. PERFORMING ORG. REPORT NUMBER SAI-76-507-BOS
7. AUTHOR(s) Harold J. Linnerud		8. CONTRACT OR GRANT NUMBER(s) DNA 001-76-C-0109
9. PERFORMING ORGANIZATION NAME AND ADDRESS Science Applications, Inc. 3 Preston Court Bedford, Massachusetts 01730		10. PROGRAM ELEMENT, PROJECT, TASK AREA & WORK UNIT NUMBERS Subtask Y99QAXSA001-78 Subtask Y99QAXSC002-01
11. CONTROLLING OFFICE NAME AND ADDRESS Director Defense Nuclear Agency Washington, D.C. 20305		12. REPORT DATE 29 December 1976 13. NUMBER OF PAGES 68
14. MONITORING AGENCY NAME & ADDRESS*(if different from Controlling Office)*		15. SECURITY CLASS. *(of this report)* UNCLASSIFIED 15a. DECLASSIFICATION/DOWNGRADING SCHEDULE

16. DISTRIBUTION STATEMENT *(of this Report)*

Approved for public release; distribution unlimited.

17. DISTRIBUTION STATEMENT *(of the abstract entered in Block 20, if different from Report)*

18. SUPPLEMENTARY NOTES

This work sponsored by the Defense Nuclear Agency under RDT&E RMSS Codes B344076464 Y99QAXSA00178 and B34407T464 Y99QAXSC00201 H2590D.

19. KEY WORDS *(Continue on reverse side if necessary and identify by block number)*

MIDDLE GUST
Ejecta
Cratering

20. ABSTRACT *(Continue on reverse side if necessary and identify by block number)*

In-flight of crater ejecta are summarized for the MIDDLE GUST test series. Observed distributions tend to support power law distribution currently used in models when the latter are filtered by gravitational and acrodynamic effects. The feasibility of obtaining data on ejecta dynamics to correlate with cratering calculations is reviewed.

403977

DD FORM 1 JAN 73 1473 EDITION OF 1 NOV 65 IS OBSOLETE

UNCLASSIFIED

SECURITY CLASSIFICATION OF THIS PAGE *(When Data Entered)*

CONTENTS

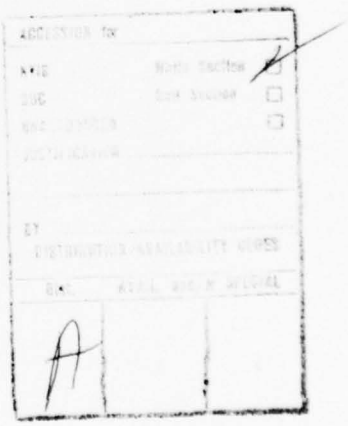

I. INTRODUCTION

Science Applications, Inc. (SAI) has been examining and predicting crater ejecta environments for both high explosive (HE) and nuclear detonations for a number of years. Supported by the Defense Nuclear Agency (DNA), SAI has developed a basic ejecta model, recently upgraded to include the latest theoretical and experimental results (see Reference 1). The work reported here is in direct support of this model development effort, and completes our efforts at characterizing the ejecta in-flight size distributions for the MIDDLE GUST series of high explosive tests.

The SAI-developed model considers the entire history of crater formation and ejecta deposition. Crater formation and ejecta throwout are modeled and trajectories of representative ejecta are calculated to provide a description of the airborne ejecta cloud. The cloud is followed to impact, and a final ejecta blanket thickness is obtained by integrating all of the ejecta impacting the surface. The final ejecta blanket is generally characterized as having two distinctly different zones. An inner zone which can be described as having a continuous distribution of ejecta material which completely covers the surface, and an outer zone where impact becomes less numerous, the covering is discontinuous, and impact assessments are best handled in a probabilistic manner.

The work reported here obtained in-flight ejecta size distributions from photographic records of the MIDDLE GUST events. Combustion products (smoke) and large amounts of lofted dust tend to obscure that part of the ejecta cloud closest to detonation. For this reason these results

are more properly correlated with the ejecta found in the outer impact zone, and then only for the larger ejecta as the limiting resolution of the photographic recording system will not permit the observation of ejecta below a certain size limit.

The following two sections of this report will outline the size distribution description used in the ejecta model, will review the supporting data for it, and will then report on the size distributions measured for the MIDDLE GUST events. The report concludes with a brief review of ejecta ballistics and the techniques used in deriving dynamic ejecta parameters such as velocity, position, drag coefficient and ejection angle from simple photographic records.

II. EJECTA SIZE MODEL AND PAST MEASUREMENTS

The SAI ejecta model has two main elements -- the crater source and a trajectory calculation. The crater source is defined by a theoretical velocity distribution for the continuous hydrodynamic material leaving the crater, by empirical models for ejecta mass, ejecta size distribution and maximum ejecta size, and by experimental observations of ejecta velocity (for high explosive shots). The trajectory calculation follows the ejecta produced by the source and, using a compressible flow aerodynamic drag model, tracks them through a flowfield defined by the VORDUM (vortex dust model) program. Using this approach we are able to characterize both the airborne ejecta cloud and the ground deposition.

The work reported here has been directed specifically at that element of the model which covers a description of ejecta size distributions. This is an important part of the ejecta model, and is currently based on an early review (Reference 2) of many different sources of ejecta -- conventional and nuclear detonations, hypervelocity impact studies, meteor impacts, etc. For cohesive media such as clay, basalt and granite, the differential mass density distribution is assumed to be represented by

$$\frac{\partial M}{\partial a} = \frac{0.5 M_e}{\sqrt{a_m}} \; a^{-0.5} \qquad (1)$$

where $\partial M/\partial a$ is the ratio of the differential mass δM associated with the differential ejecta diameter δa, a_m is the diameter of the largest ejecta, and M_e is the total ejecta mass in megatons. This relationship is used

over a range of ejecta sizes from 10^{-4} to 1 meter, and Gault, et al (Reference 3) compiled data for explosive and impact cratering events to derive a correlation of mass of largest ejecta (M_m) with M_e as

$$M_m = 6.6 \times 10^5 \, M_e^{0.8} \tag{2}$$

(M_m in kg) over 14 orders of magnitude variation in M_e. Assuming that the ejecta can be represented as spherical (a good assumption as was shown in Reference 4), then $M_m = \pi \rho a_m^3/6$ and the above relationship would imply that

$$\frac{\partial N}{\partial a} \propto a^{-3.5} \tag{3}$$

where $\partial N/\partial a$ is the ejecta differential number density as a function of size. With the upper limit of a_m, Equation 1 is assumed valid for all cratering media except those specifically identified as alluvial or sand with water table levels below the apparent crater depth. For the latter media, Reference 2 suggests a more accurate relationship of the form

$$\frac{\partial M}{\partial a} = \frac{M_e}{a} \, . \tag{4}$$

The maximum ejecta diameter for such soils is likely to be best equated with maximum in-situ diameter (rather than M_e), and this diameter is employed as the upper limit in Equation 4.

The experimental data upon which the above two power laws are based generally falls into two classes. First, there are post-shot observations made by direct retrieval of impacting ejecta or by making secondary estimates based upon size of ejecta impact craters or upon accumulation of all ejecta debris. Figure 1 is a typical summary of

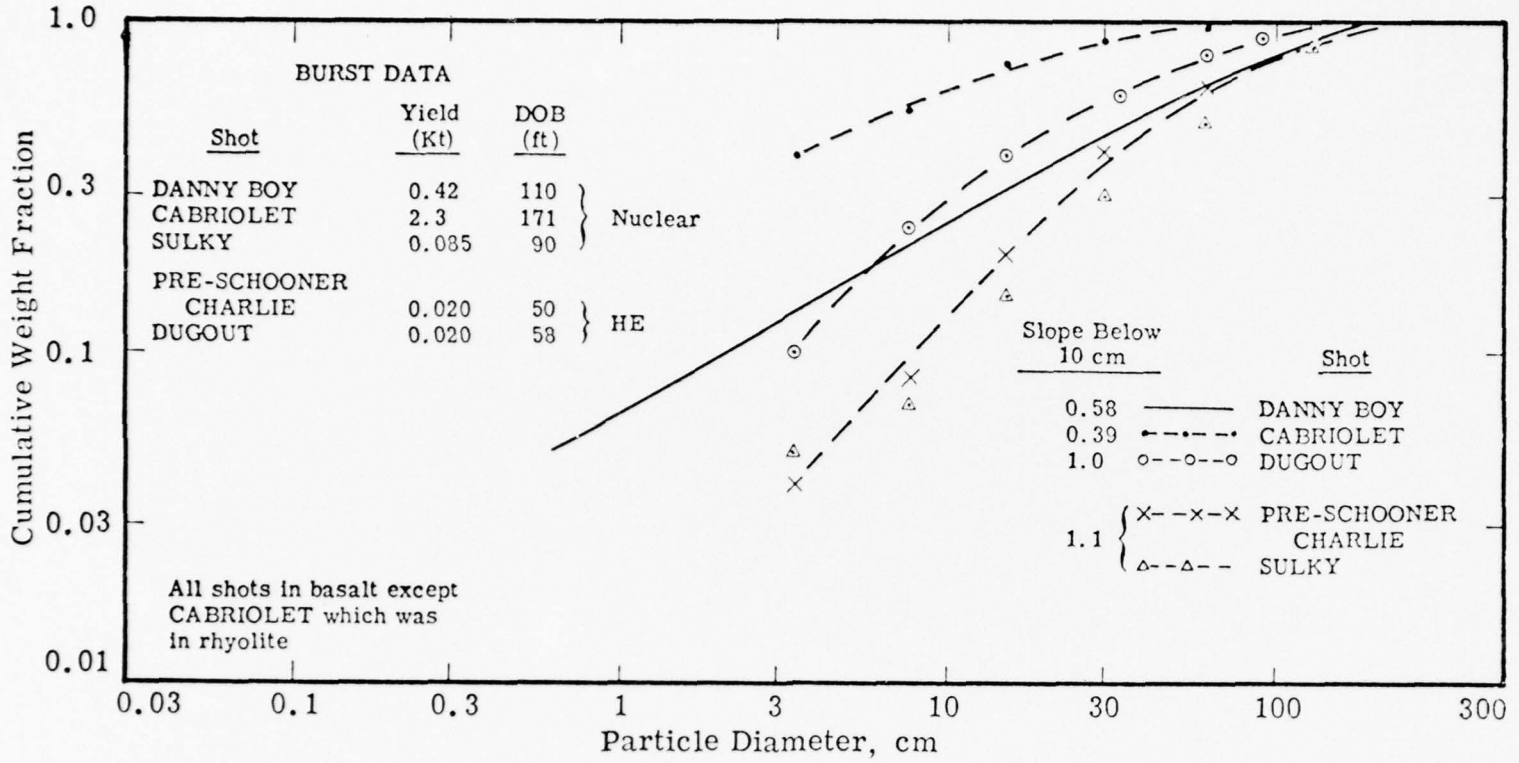

Taken from Reference 5

Figure 1 Size Distributions for Five NTS Shots

such data. Second, observations have been made by in-situ sampling of the smaller ejecta (dust) which are lofted and held up by the convective forces surrounding the rising fireball (see Figure 2). Neither of these techniques are direct observations of in-flight characteristics for larger ejecta, and a different approach was sought which would provide such information and hopefully validate the use of the above power laws.

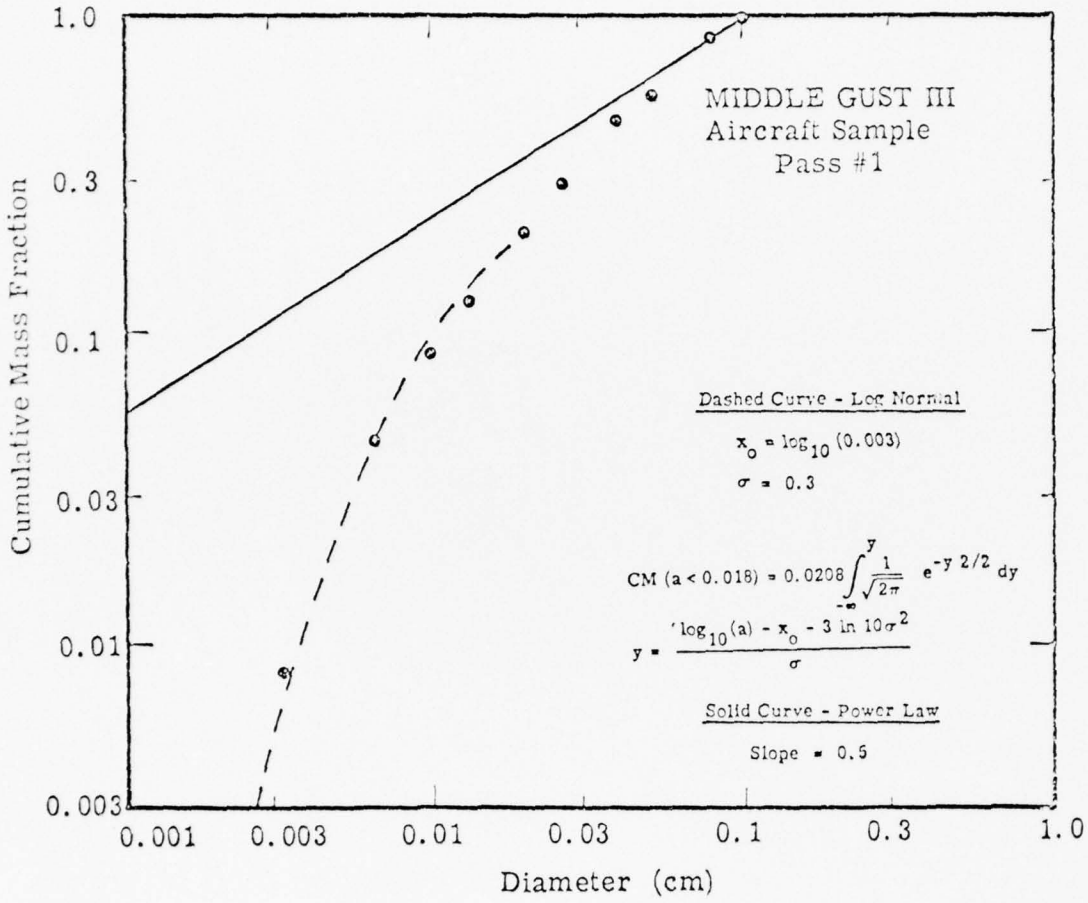

Taken from Reference 5

Figure 2 MIDDLE GUST III Size Distribution

III. EJECTA SIZING FOR THE MIDDLE GUST EVENTS

The Denver Research Institute (DRI), under contract to DNA, has been tasked with obtaining documentary and technical photography of almost all of the high explosive tests which DNA has supported. Of specific interest are the higher framing rate records which have been utilized by DRI in obtaining fireball and dust cloud dimensional measurements and subsequent drift rates, and in those records which were obtained with exposure times and spatial resolutions sufficient to obtain dynamic parameters for the crater ejecta. The latter records were exposed to permit dimensional measurements with enough accuracy to allow the estimation of ejecta velocity, ejection and impact angles, and of drag coefficient. Coincidentally, these records provide fairly wide field "snapshots" of the airborne ejecta cloud which can be used to quantize in-flight size distributions (see Reference 6 for a detailed description of the photography, and of the analysis techniques employed by DRI).

Obtaining statistically meaningful data from these records is simple enough in concept, but difficult in practice. A direct frontal assault would imply the utilization of a magnifying lens on the original imagery and/or controlled enlargements of selected frames to make manual observations of the ejecta sizes. This is obviously a tedious and error-prone way to proceed, and it was determined that an image analysis system (specifically

the IMANCO Quantimet) could perform the necessary sizing and analysis task (see Reference 7) with a minimum of observer discomfort and with increased accuracy and throughput. An initial analysis started with two of the larger shots (20 and 100 ton) of the MIDDLE GUST high explosive test series (see References 4 and 8) and the work reported here continues with ejecta sizing for other, lower yield, events of that same series.

The events analyzed in References 4 and 8 were MIDDLE GUST I, a 20 ton half-buried sphere of TNT, and MIDDLE GUST III, a 100 ton tangent-above sphere of TNT. Qualitatively, these two shots yielded in-flight sizing data, shown in Figure 3, which was similar. The $a^{-3.5}$ power law curve superimposed on these measured curves might, at first glance, imply that the use of such a power law in the ejecta model is questionable. To resolve this, the ejecta model was exercized for the 100 ton event and the airborne ejecta field at 5 seconds was mapped in detail. That portion of the ejecta field which coincided with the field-of-view of DRI's recording cameras was isolated and numerically summed to create a size distribution curve which was directly comparable to the measured data. These results are shown in Figure 4 where it can be seen that there is reasonable agreement between the prediction and the experimental observations. It should be noted that at least some of the flattening of the experimental curve, for smaller ejecta, is due to resolution problems associated with the recording systems (film and camera) and with the image analysis system (see Reference 4).

With such general validations of the power law size distribution in the ejecta model, it was thought appropriate to extend such experimental observations to other geologies. The calibration shots for the MIDDLE

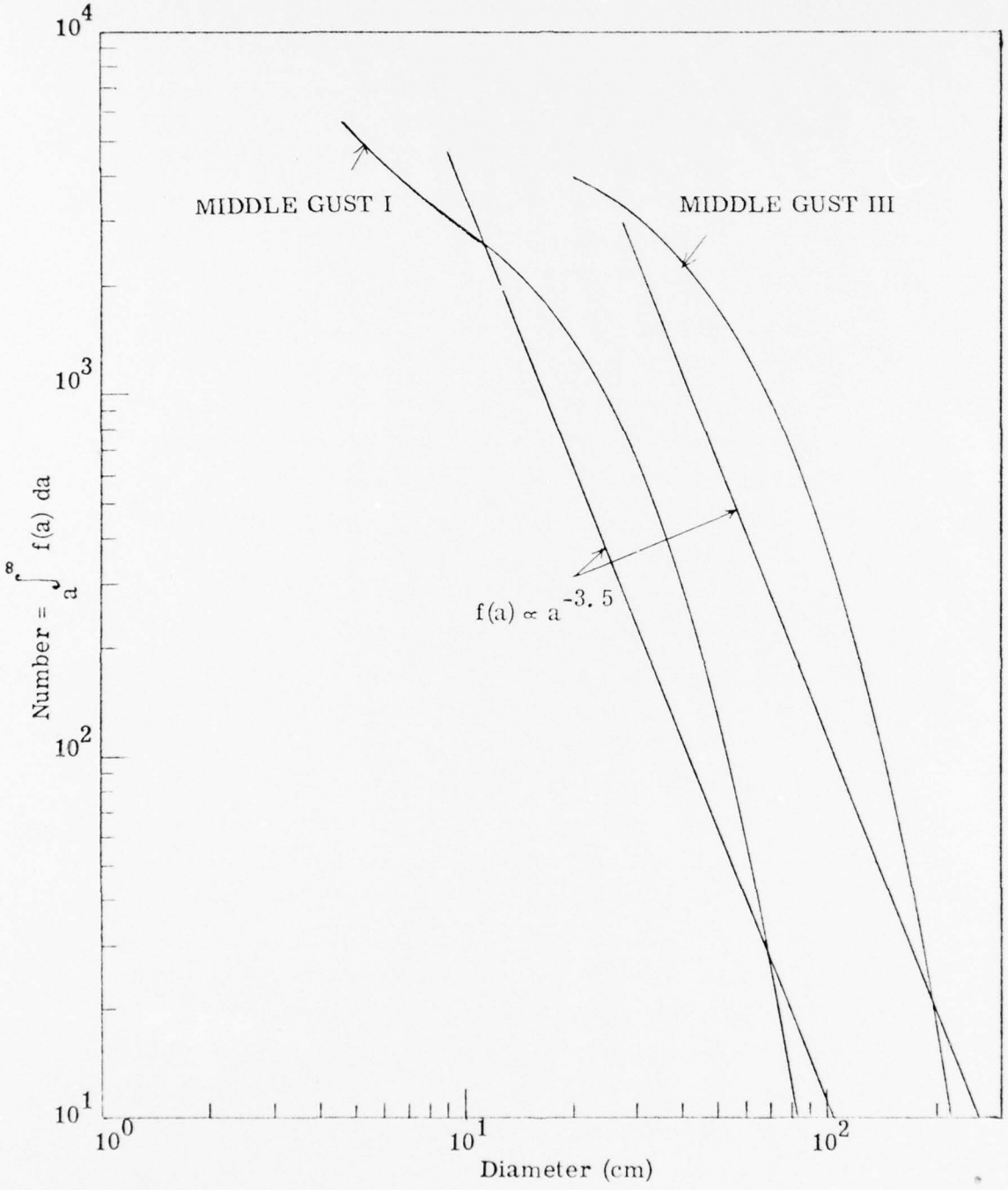

Figure 3 Averaged Size Distributions for MIDDLE GUST I and III

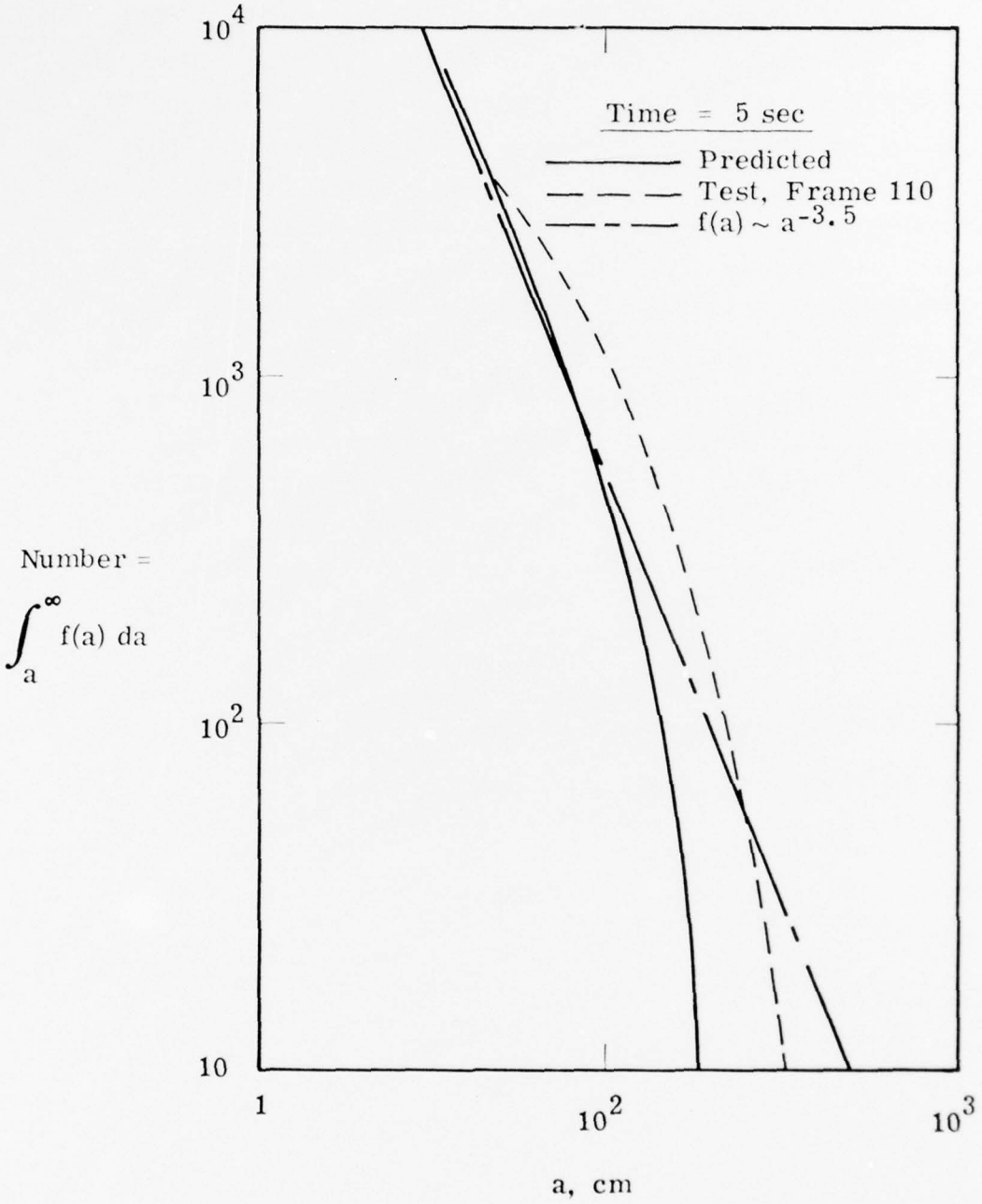

Figure 4 Integral Ejecta Fragment Counts - 100-Ton Bursts

GUST series were 1000 pound TNT detonations which were set off over varying sub-surface geologies. The overall geology was that for events I and III except that pre-shot excavating permitted detonations over changing sub-surface media as is shown in Figure 5. The four shots illustrated in this figure were selected for analysis because they had moderately good photographic records and because the only difference between the shots was sub-surface geology, i.e., all four shots were 1000 pound half-buried spheres of center-initiated TNT.

As for shots I and III, the calibration shots were recorded with DRI's 70mm Hulcher cameras with slight changes in range-to-detonation and in the focal length of the lenses used. The pertinent recording parameters are summarized below, but all appropriate geometric corrections have been included in the results presented.

Table 1

Pertinent Recording Parameters for MIDDLE GUST Calibration Events

Event	Camera Range (ft)	Lens Focal Length (mm)	Charge Position from Original Ground Level
3a	447	150	0
6	670	150	4
8	754	150	9
9	757	150	16

For all four shots, the airborne ejecta field was quantized at 2, 4 and 6 seconds after detonation. On the 3a event the recording cameras were considerably closer to the

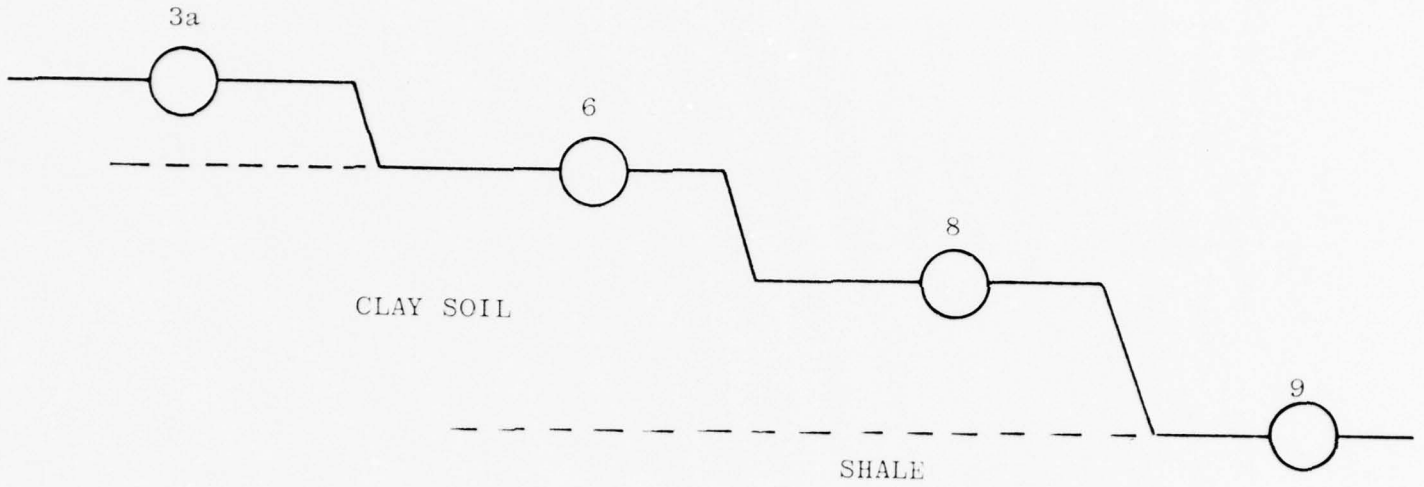

Figure 5 Relative Geometry and Geology for MIDDLE GUST Calibration Shots

detonation than for the other shots and therefore by 6 seconds after detonation much of the ejecta field has exceeded the recording cameras field-of-view and no data were acquired. Full field measurements were made, either East or West of the detonation, and several symmetry checks were made at two seconds after detonation. For all of these shots, the ejecta field had not exceeded recording bounds so that measurements generally included all ejecta, on one side, up to the edge of the fireball/dust cloud.

Figures 6 through 9 are typical of the data which were acquired in these sizing measurements. For clarity, the data points have been eliminated, and only the "eyeball" fits are shown to indicate general trends. (Data for these plots are tabulated in Appendix A.) A review of these figures will show that shots 3a, 6 and 9 have very similar size distribution curves, that the total ejecta field diminishes in time, and that the larger ejecta tend to drop out preferentially. Also, it would appear that shot 9, over a shale geology, tended to produce significantly more ejecta than either of the other two shots. Shot 8 appears to differ from the others in only one respect, that its distribution curves appear to be flatter (i.e., more larger ejecta, or fewer small ones). The reason for this is not apparent, but it was set off over a clay geology which might have biased the distribution.

Figures 10 and 11 take the two and four second curves from the preceding four figures, and combine them for direct comparison. Here the increased ejecta count for shot 9 is readily seen, particularly at two seconds where an apparent factor of two in total count is readily observed. The differential has dropped by four seconds, but shot 9 is still on the upper bound of the envelope. Also seen in these figures is the apparent flattening of the distribution for shot 8.

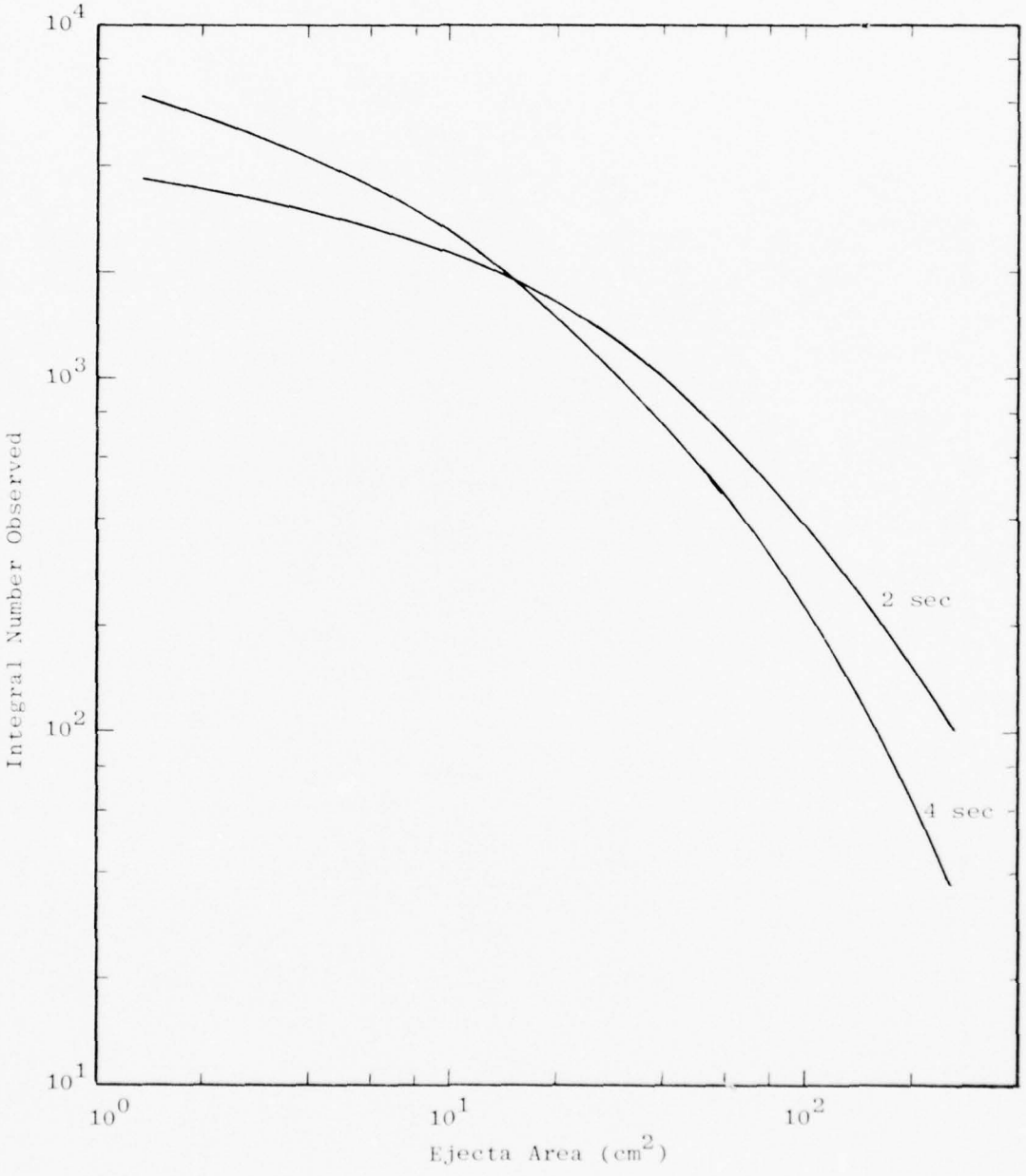

Figure 6 Ejecta Sizing for MG Calibration Shot 3a

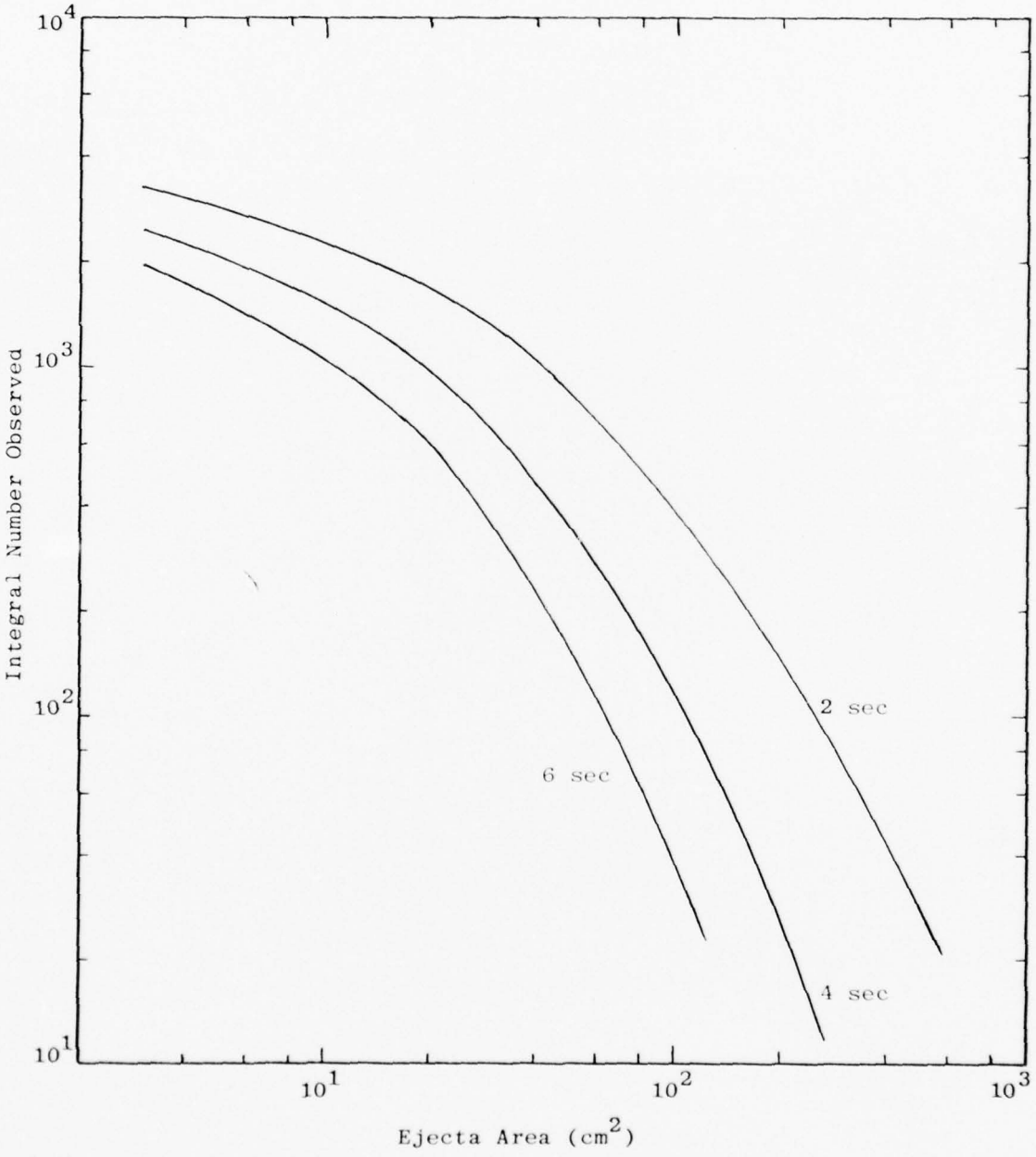

Figure 7 Ejecta Sizing for MG Calibration Shot 6

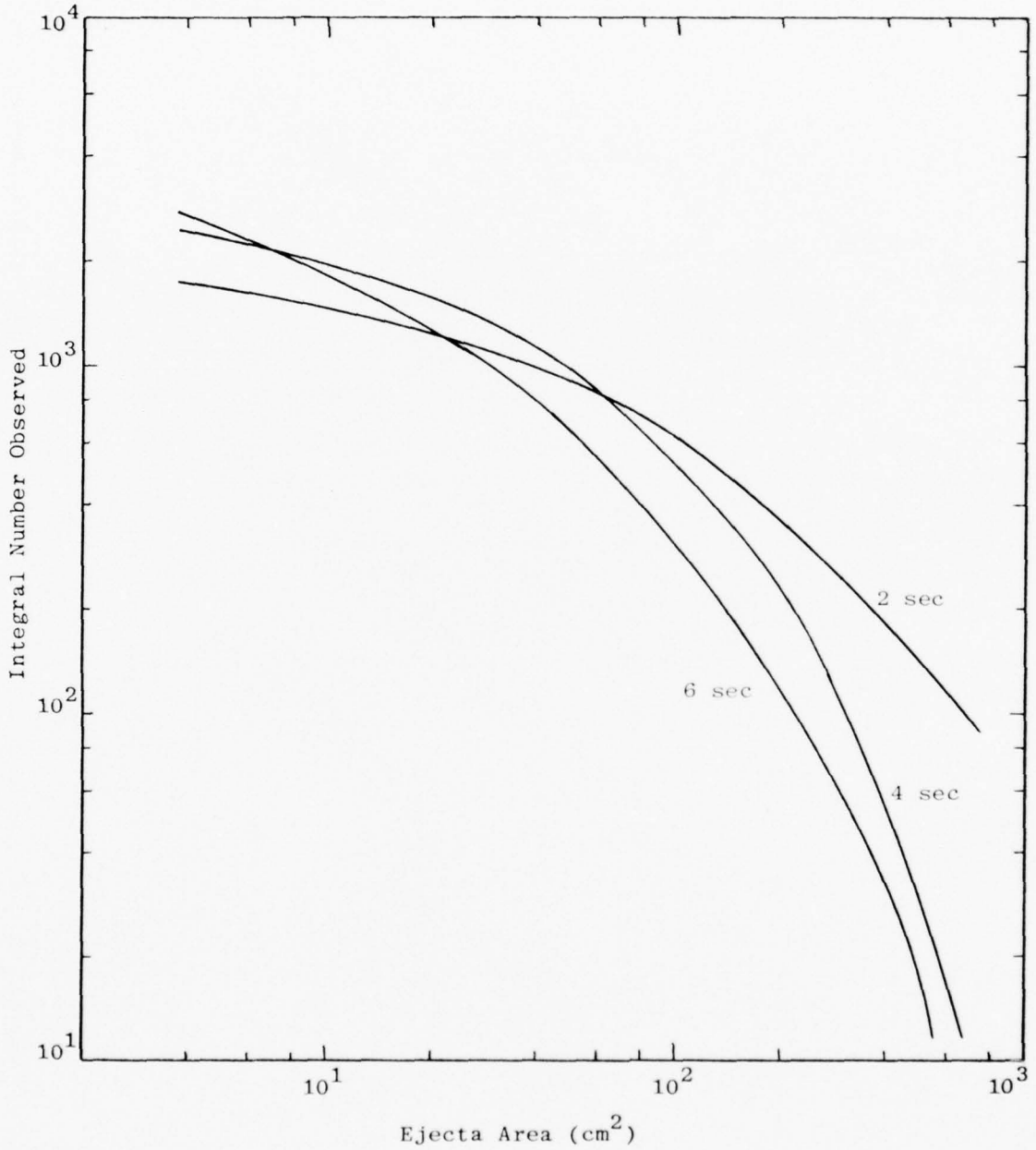

Figure 8 Ejecta Sizing for MG Calibration Shot 8

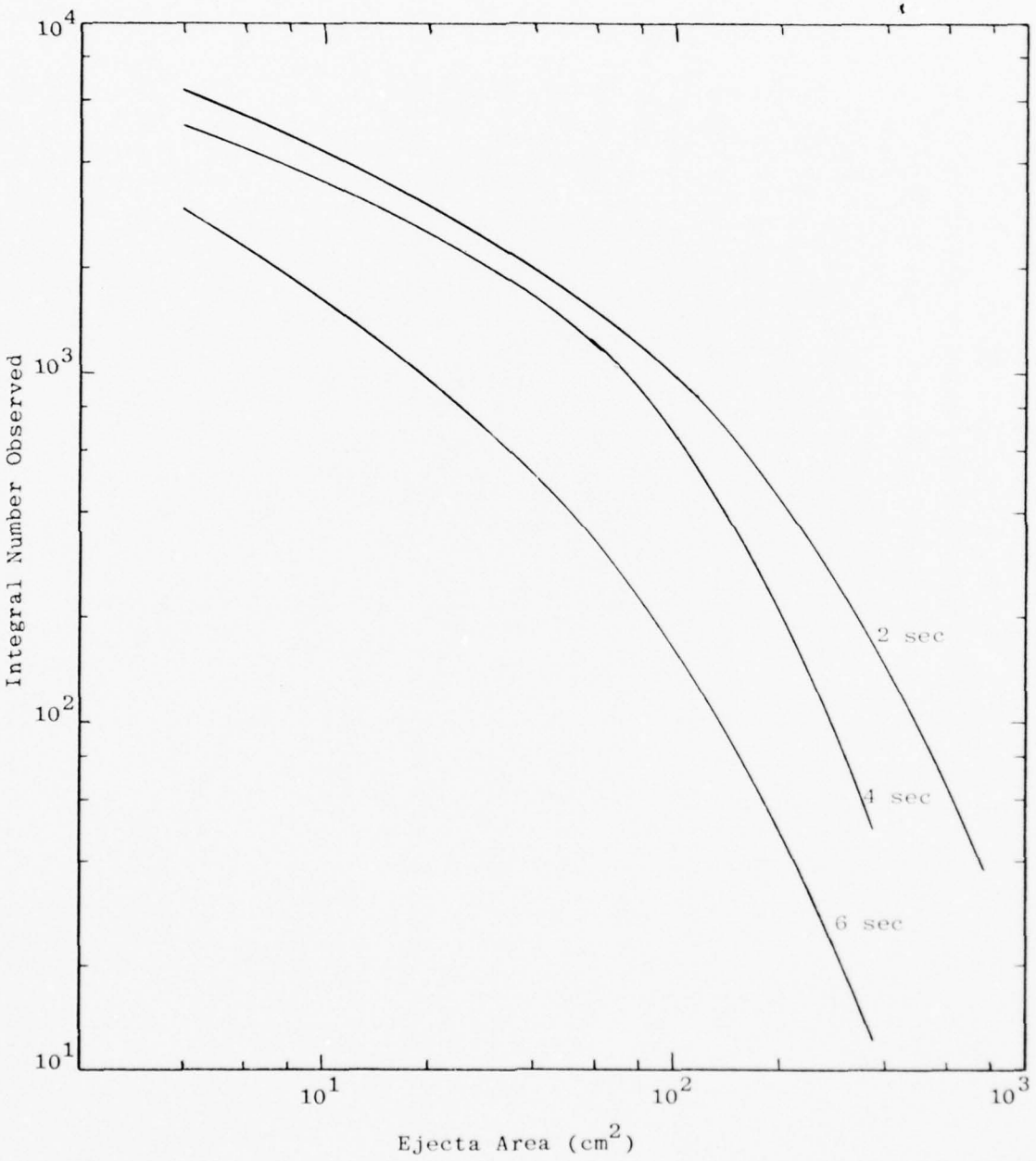

Figure 9 Ejecta Sizing for MG Calibration Shot 9

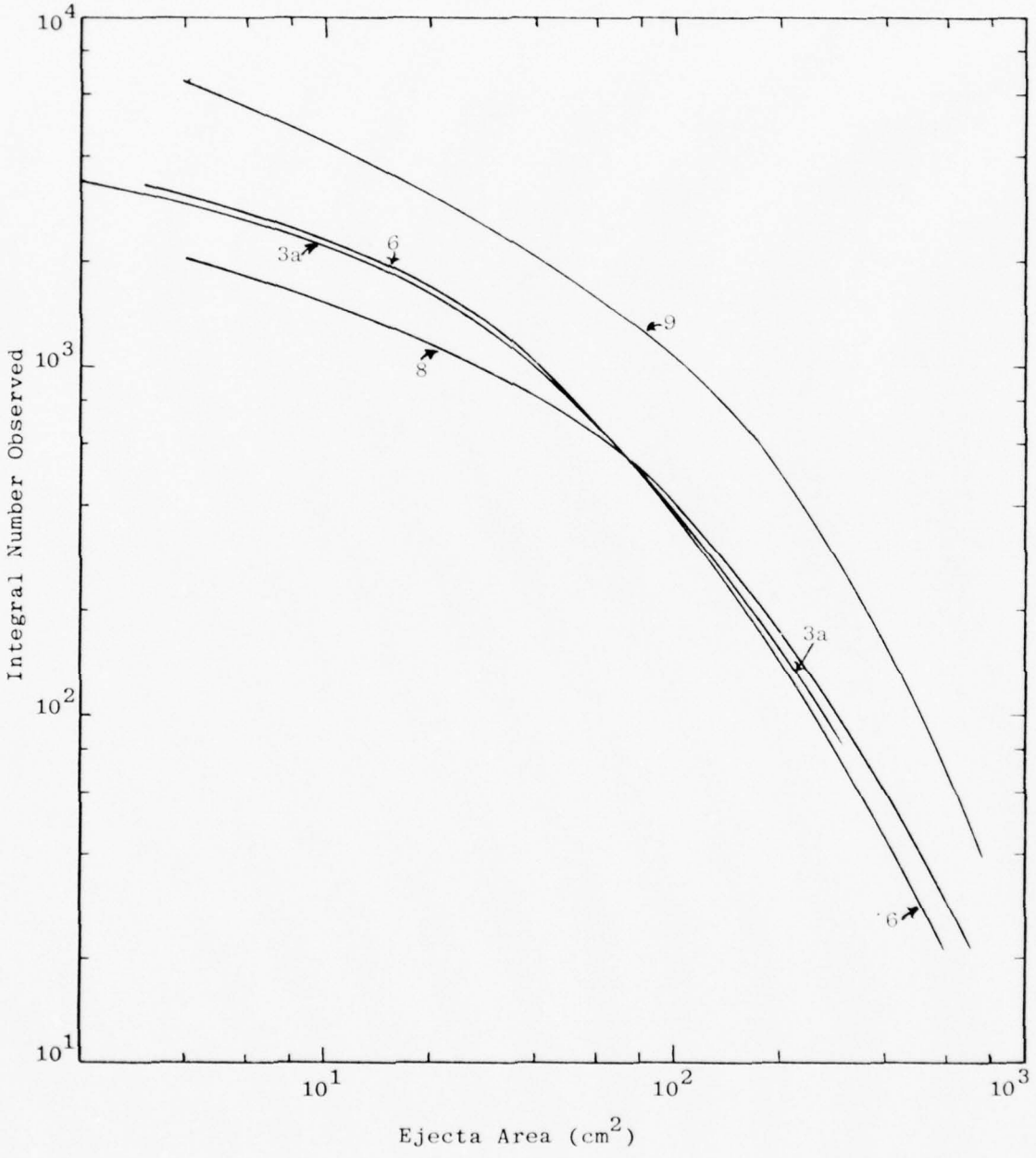

Figure 10 Comparison of Ejecta Sizing at 2 Seconds After Detonation

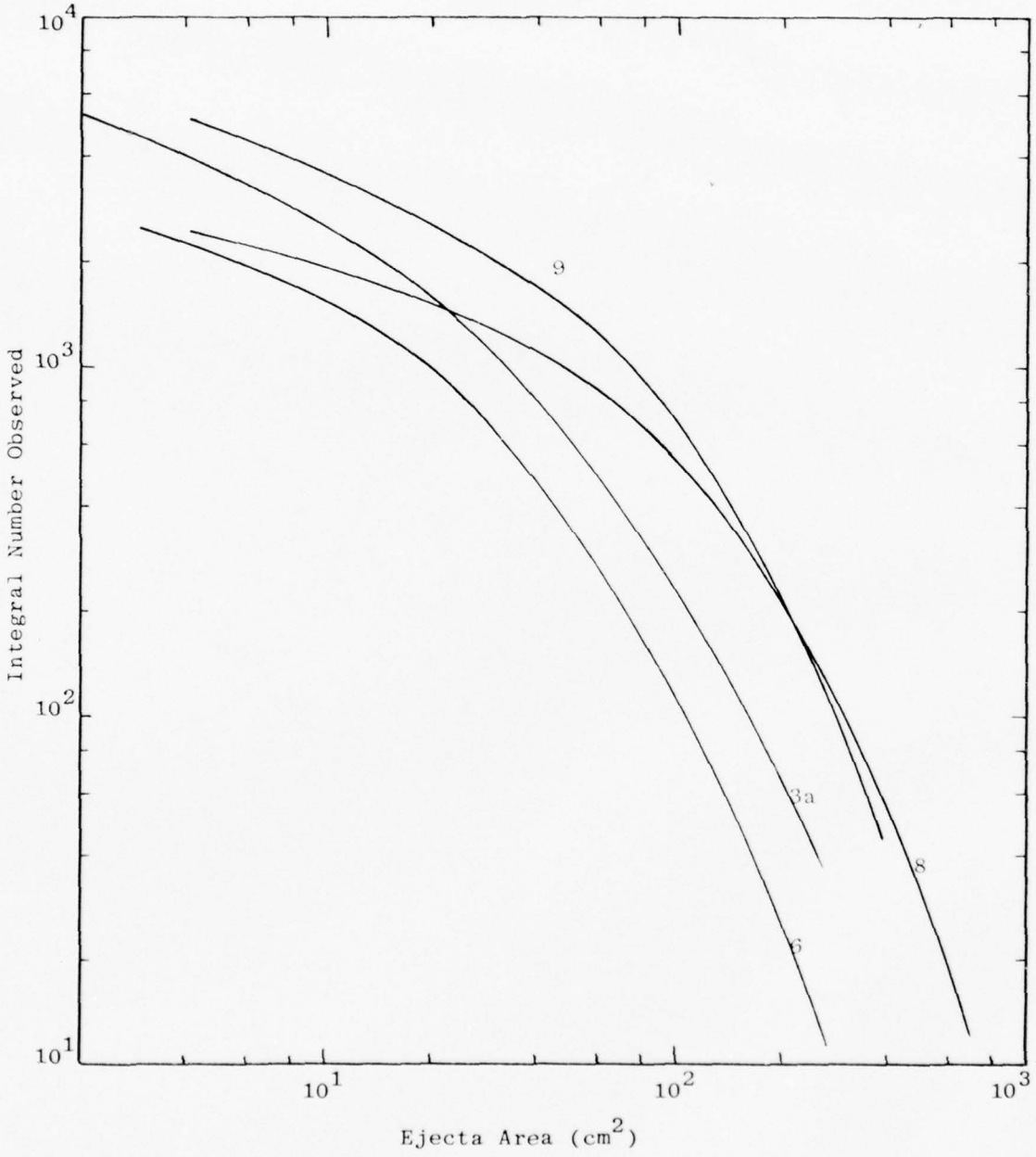

Figure 11 Comparison of Ejecta Sizing at 4 Seconds After Detonation

Figures 12, 13, and 14 compare ejecta field measurements made East and West of shots 6, 8 and 9, two seconds after detonation.* It can be seen from these figures that the events were indeed highly symmetrical and that there is no apparent biasing of the data in either of the viewing directions.

In Figure 15 we combine size distribution curves for the four calibration shots with data from the 20 and 100 ton events. The results for the calibration shots and the 20 ton shot should be directly comparable as these were all half-buried, center-initiated, spherical charges, but the 100 ton event was tangent-above and therefore not directly comparable.

*A similar comparison could not be made for shot 3a because a different film, which was underexposed, had been used on one side. It should also be noted that shots 6, 8 and 9 were recorded on Shellburst film, while 3a was recorded on tri-x panchromatic. Data presented here for the preceeding three shots are therefore directly comparable, while that for 3a might be slightly biased because tri-x does not quite have the spatial resolution capability of Shellburst.

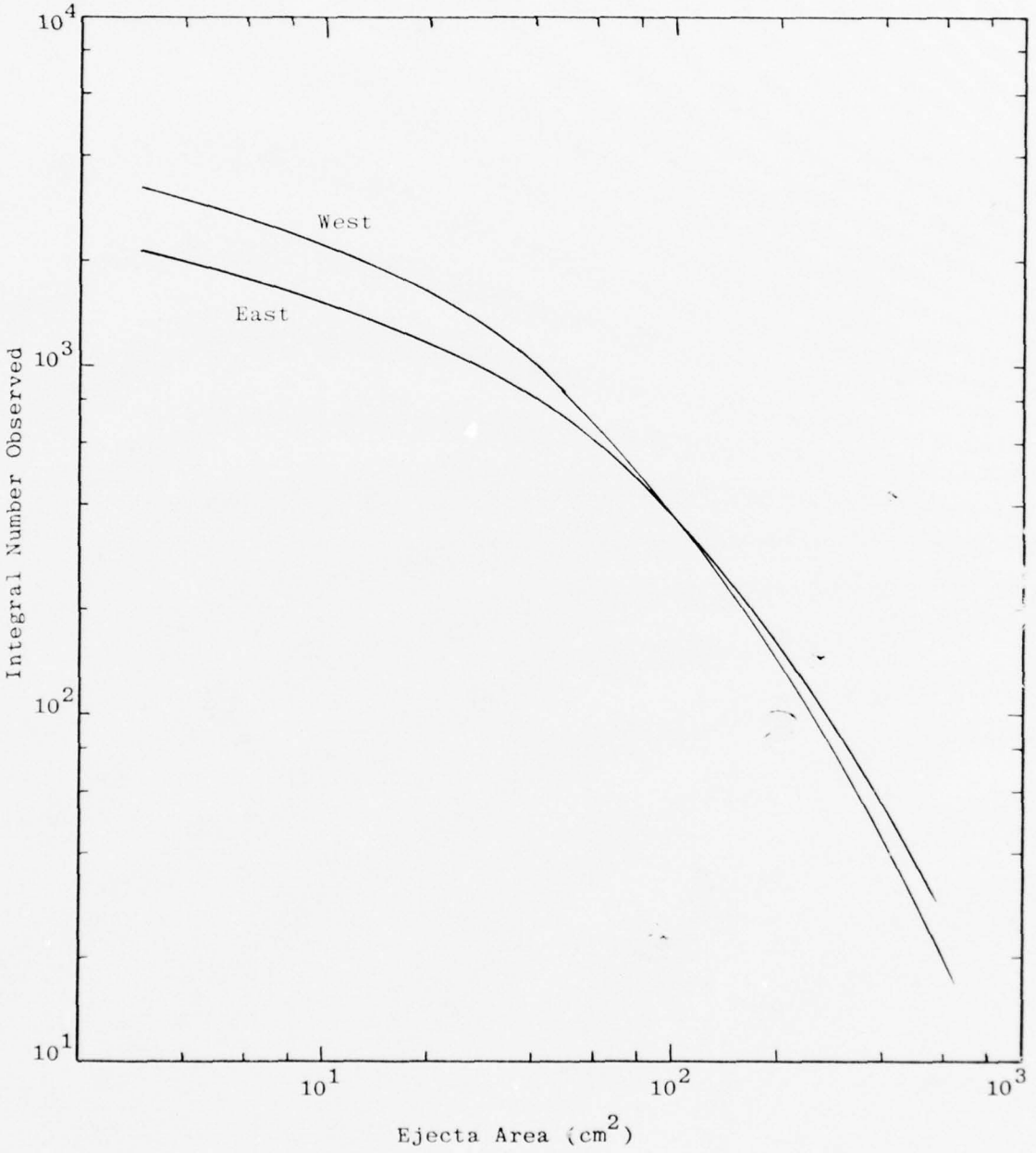

Figure 12 Symmetry Check on Shot 6 at 2 Seconds

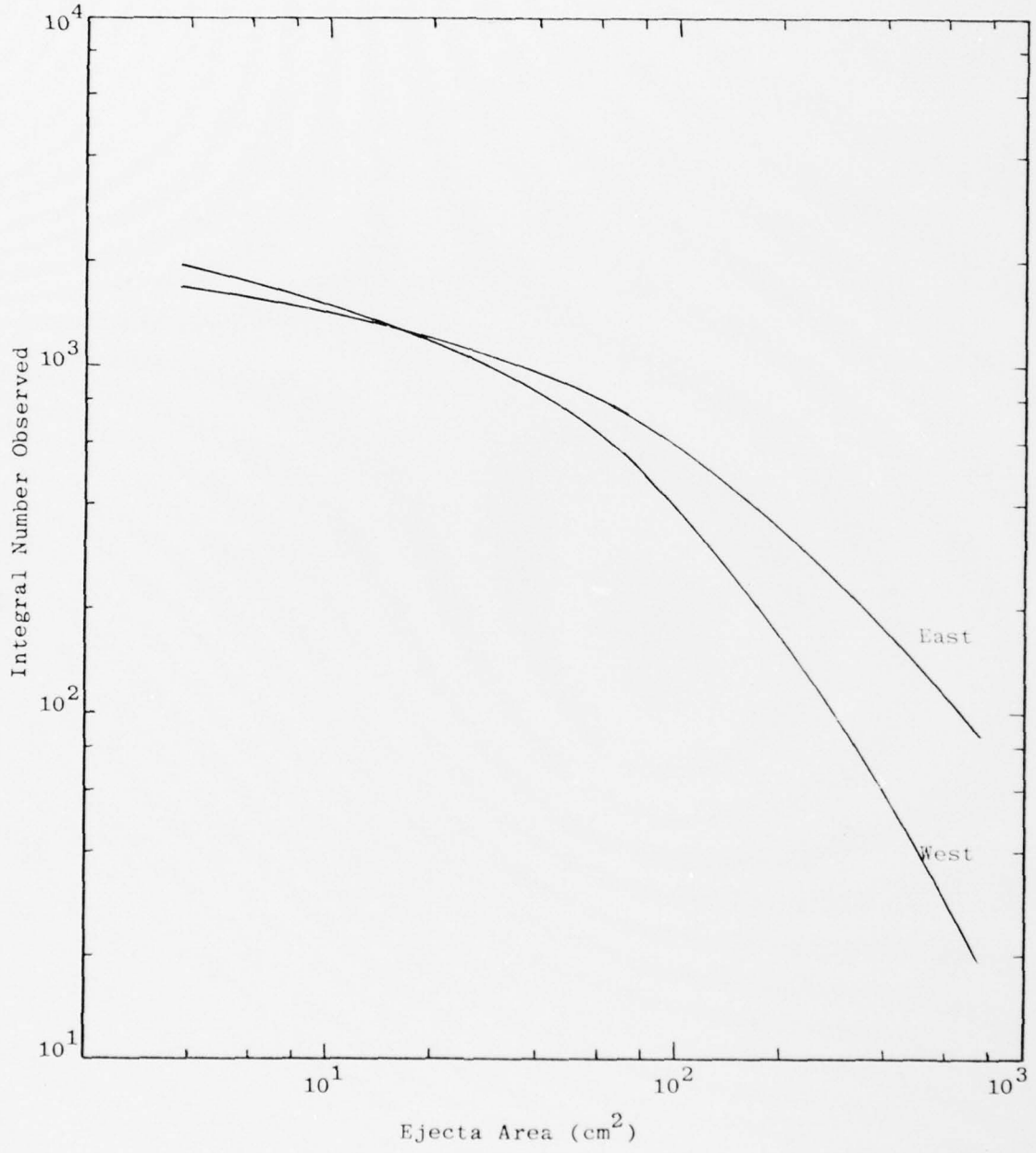

Figure 13 Symmetry Check on Shot 8 at 2 Seconds

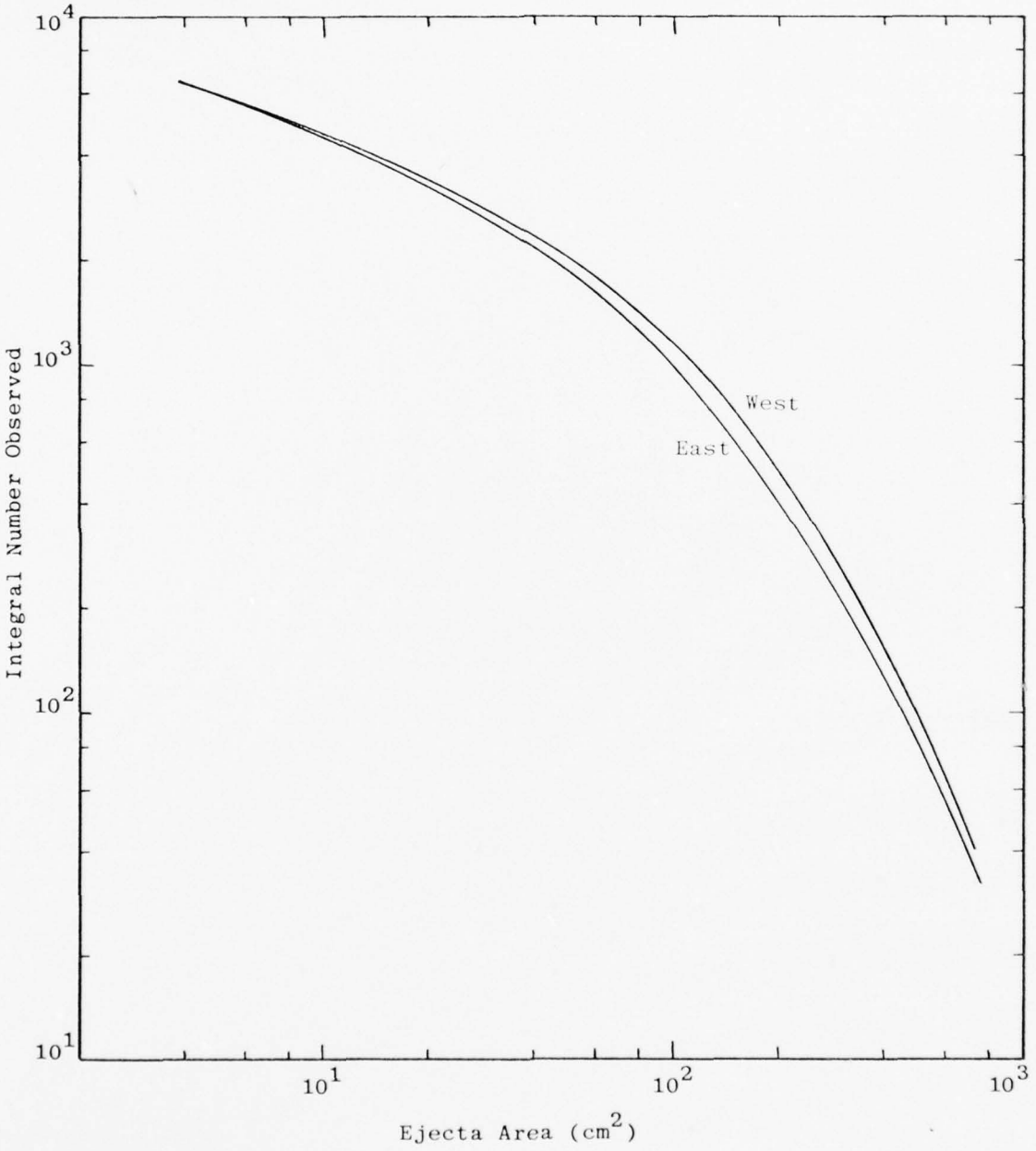

Figure 14 Symmetry Check on Shot 9 at 2 Seconds

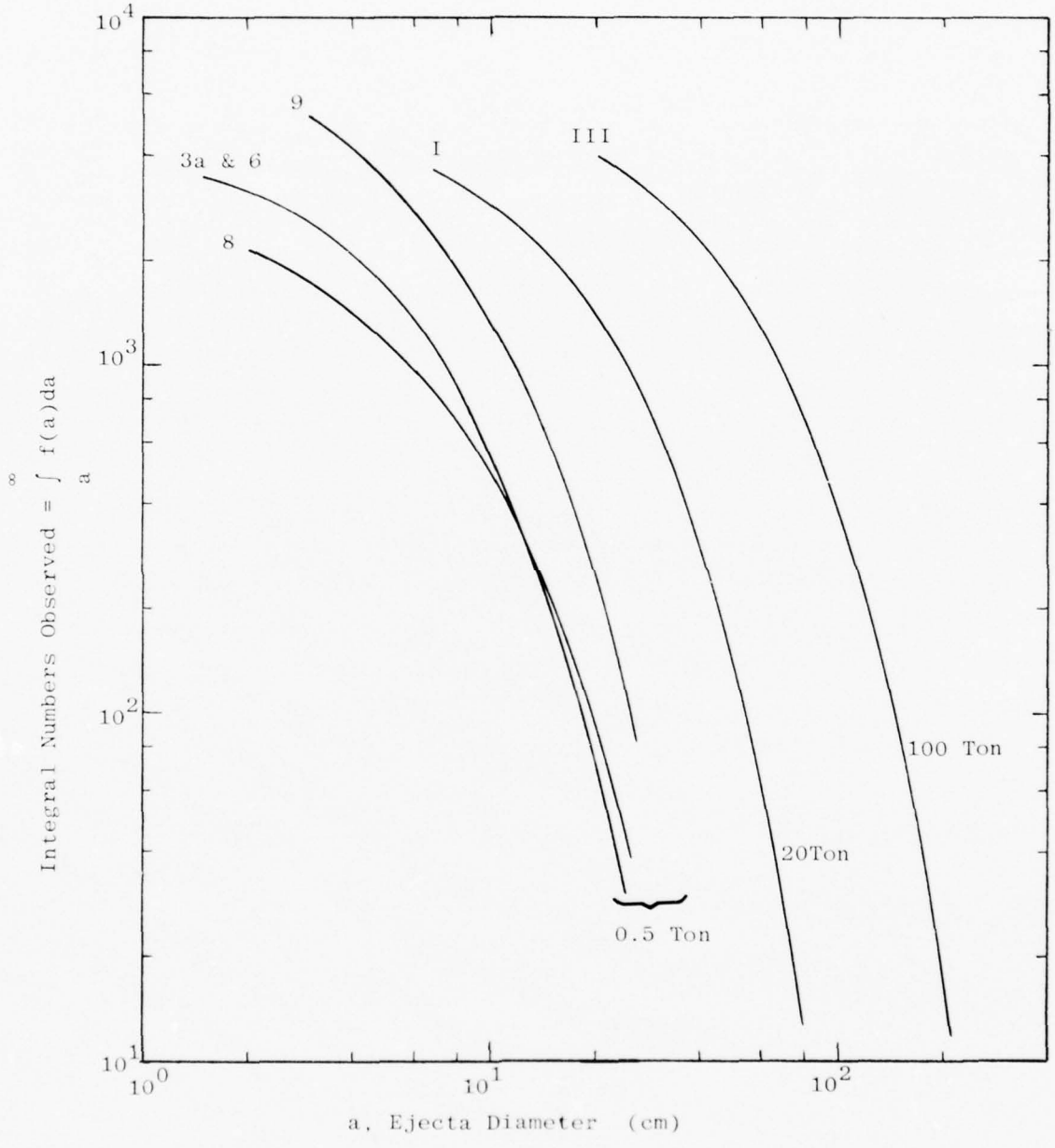

Figure 15 Comparison of Ejecta Sizing for MIDDLE GUST Events at Approximately 2 Seconds

IV. DETERMINATION OF EJECTA DYNAMICS FROM PHOTOGRAPHICALLY RECORDED TRAJECTORIES

One of the main objectives of the DRI photographic projects is to obtain data on ejecta dynamics. Originally, these investigations were limited to in-flight and impact parameters, but as the SAI ejecta model was developed an additional need for quantitative ejection parameters evolved. To obtain the desired data DRI has developed an analysis program which uses trajectory coordinates obtained from digitized photographic records (Reference 9).

Ejection velocities initially reported by DRI were inconsistent with values being used in the ejecta model and implied impact ranges which were considered too long. A critical review of the DRI analysis procedure revealed several defects, and their approach has recently been improved to provide more reasonable and accurate ejection parameters (Reference 6). However, the ejecta are expelled from the crater at some azimuthal angle (i.e., toward or away from the recording camera) and determination of this angle from the recorded trajectory remains uncertain at best. SAI was asked to review trajectory analysis techniques and to determine an optimum approach (if any) to measure this angle and therefore to improve the accuracy of estimated dynamic parameters.

The coupled differential equations of motion which describe (in the trajectory plane) ballistic trajectories for ejecta are given by

$$\ddot{x} = d^2x/dt^2 = -\frac{K}{2}\sqrt{(dx/dt)^2 + (dy/dt)^2}\, dx/dt \qquad (5)$$

and

$$\ddot{y} = d^2y/dt^2 = -\frac{K}{2}\sqrt{(dx/dt)^2 + (dy/dt)^2}\ dy/dt - g \qquad (6)$$

where

x,y = horizontal and vertical trajectory coordinates
g = gravity
K = drag force = $\rho C_D A/m$

and

ρ = atmospheric density
C_D = drag coefficient
A = projected ejecta area
m = ejecta mass.

These equations may be used to analyze ejecta trajectories by assuming no ablation or agglomeration for the ejecta, and by assuming some simple model for C_D (e.g. constant). Note that in the absence of drag these equations reduce to those describing a simple parabolic trajectory, and near trajectory peak these equations again reduce to a simpler form. Near peak, y is maximum and $dy/dt \simeq 0$. Then

$$\frac{d^2x}{dt^2} = \frac{du}{dt} = -\frac{K}{2}\left(\frac{dx}{dt}\right)^2 = -\frac{K}{2}\,u\,\frac{dx}{dt} \quad . \qquad (7)$$

Rewriting we have

$$\frac{du}{u} = -\frac{K}{2}\,dx \qquad (8)$$

and integrating,

$$u(x_2) = u(x_1)\ \exp\left[-\frac{K}{2}\,(x_2 - x_1)\right] \quad . \qquad (9)$$

Near the trajectory peak, then, the horizontal velocity component is degraded exponentially according to Equation 9. Note that the above equations can at most yield K, and that a value for C_D will depend on the accuracy with which ejecta dimensions may be measured.

To correctly interpret photographically recorded ejecta trajectories, specifically to obtain ejection, impact and dynamic parameters, requires a detailed understanding of imaging optics and the geometric relations of the image plane, the plane-of-view, and the trajectory plane. Figures 16 and 17 are schematic representations of the image plane (film) and the plane-of-view (note that we have here corrected the left-to-right and top-to-bottom inversion created in the image plane). The image (film) plane is readily understood, but we now define the plane-of-view as that plane perpendicular to the camera's optic axis and passing through the detonation point (GZ). This is the simplest plane to make measurements in, and the distance from camera to plane, along the optic axis, is called the Range on Optic Axis (ROA).

In general, the distance from camera to GZ (the range, R) is known, as is the camera aiming in terms of elevation and azimuthal angles (El and Az) with respect to GZ. R and ROA are then related with the simple expression

$$R = ROA\ (1 + \tan^2 El + \tan^2 Az)^{\frac{1}{2}} . \qquad (10)$$

Also, measurements on the film (d) are directly related to distances in the plane of view (D) by

$$D = md, \qquad (11)$$

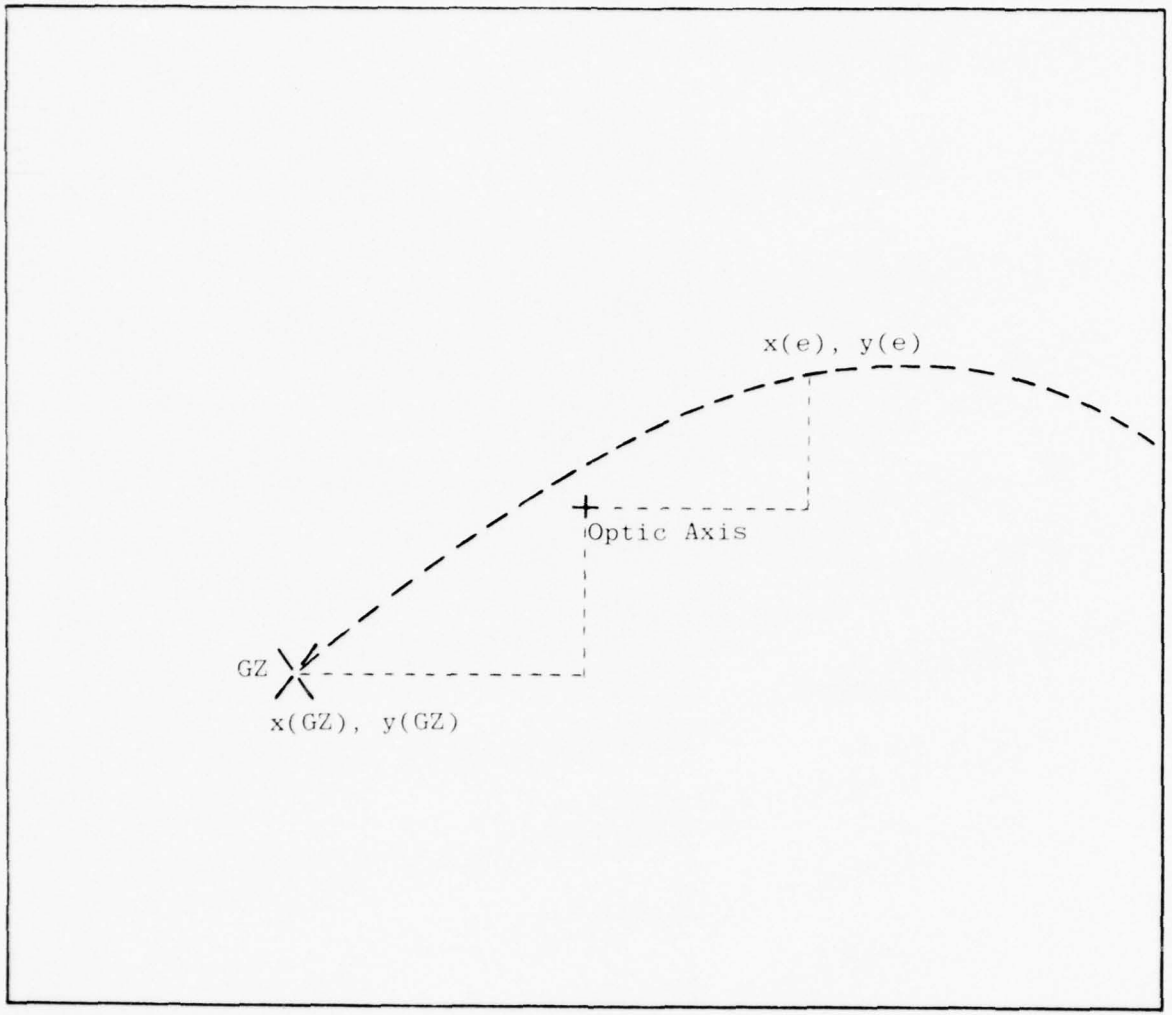

Figure 16 Outline of Digitized Ejecta Trajectory

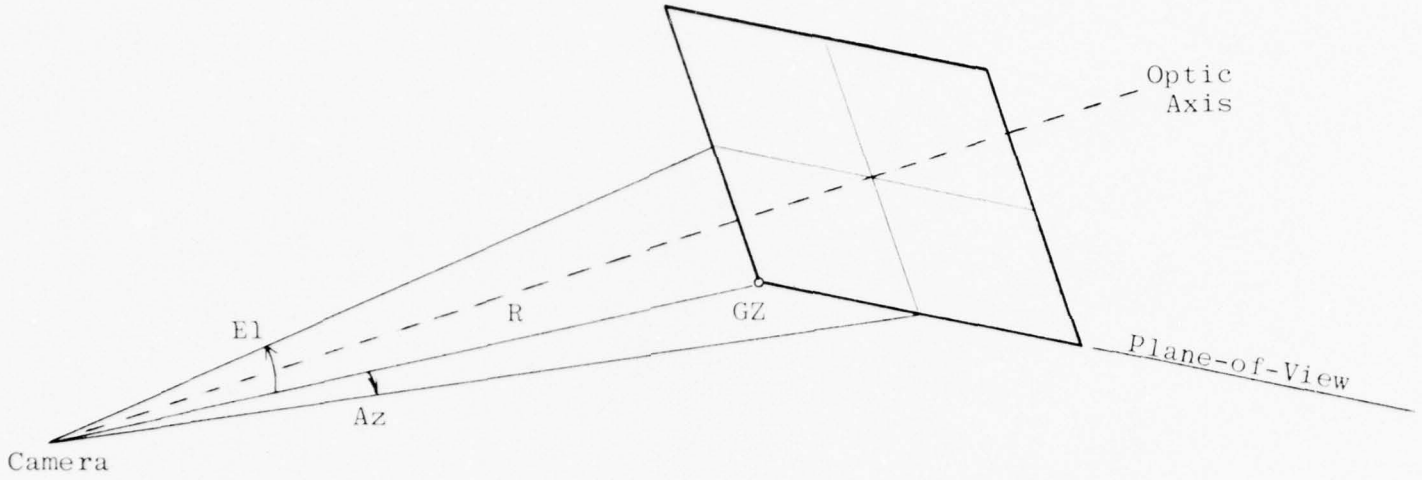

Figure 17 Outline of Camera, GZ and Plane-of-View

where m, the magnification factor, is defined by

$$m = ROA/f, \tag{12}$$

and f is the focal length of the camera lens. Note also that Az and El may be readily obtained from film measurements of the x and y displacements of GZ from the optic axis as

$$\tan El = y(GZ)/f \tag{13}$$

and

$$\tan Az = x(GZ)/f. \tag{14}$$

ROA is then calculated with Equation 10.

It is now noted that ejecta measurements in the film plane, x(e) and y(e), can be projected onto the plane-of-view and that azimuthal and elevation angles may be ascribed to the ejecta with respect to the optic axis and the direction vector to GZ. The latter is essentially horizontal, and we use this fact and the derived azimuth and elevation angles to determine ejecta location in the trajectory plane.

Referring to Figure 16, the center "+" is meant to represent the optic axis of the recording system. The elevation and azimuth angles of GZ with respect to the optic axis are defined by

$$El(GZ) = \tan^{-1}\left[\frac{y(GZ)}{f}\right] \tag{15}$$

and

$$Az(GZ) = \tan^{-1}\left[\frac{x(GZ)}{f}\right]. \tag{16}$$

Similarly, the El and Az of the ejecta with respect to the optic axis are defined by

$$El(e) = \tan^{-1} \frac{y(e)}{f} \quad (17)$$

and

$$Az(e) = \tan^{-1} \frac{x(e)}{f} \quad (18)$$

The desired angles θ and ϕ are then simply given by

$$\theta = El(e) - El(GZ) \quad (19)$$

and

$$\phi = Az(e) - Az(GZ). \quad (20)$$

This is illustrated in Figure 18 where the azimuth and elevation angles have been labeled ϕ and θ, respectively, and the ejecta plane has been rotated by an angle β with respect to a vertical plane perpendicular to the line between camera and GZ. The angle β itself is not of interest, but its knowledge is necessary to correctly calculate the x,y position of ejecta in the trajectory plane.

With the aid of Figure 18, the following relationships are readily derived to determine ejecta position in the trajectory plane as a function of R, θ, ϕ, and β:

$$x = \frac{R \sin \phi}{\cos(\beta + \phi)} \quad (21)$$

$$y = \frac{R \tan \theta \cos \beta}{\cos (\beta + \phi)} \quad . \quad (22)$$

Current Analysis Technique

Details of the analysis scheme currently used to derive dynamic parameters from digitized imagery are found in Reference 6. This approach may be summarized in the following four steps:

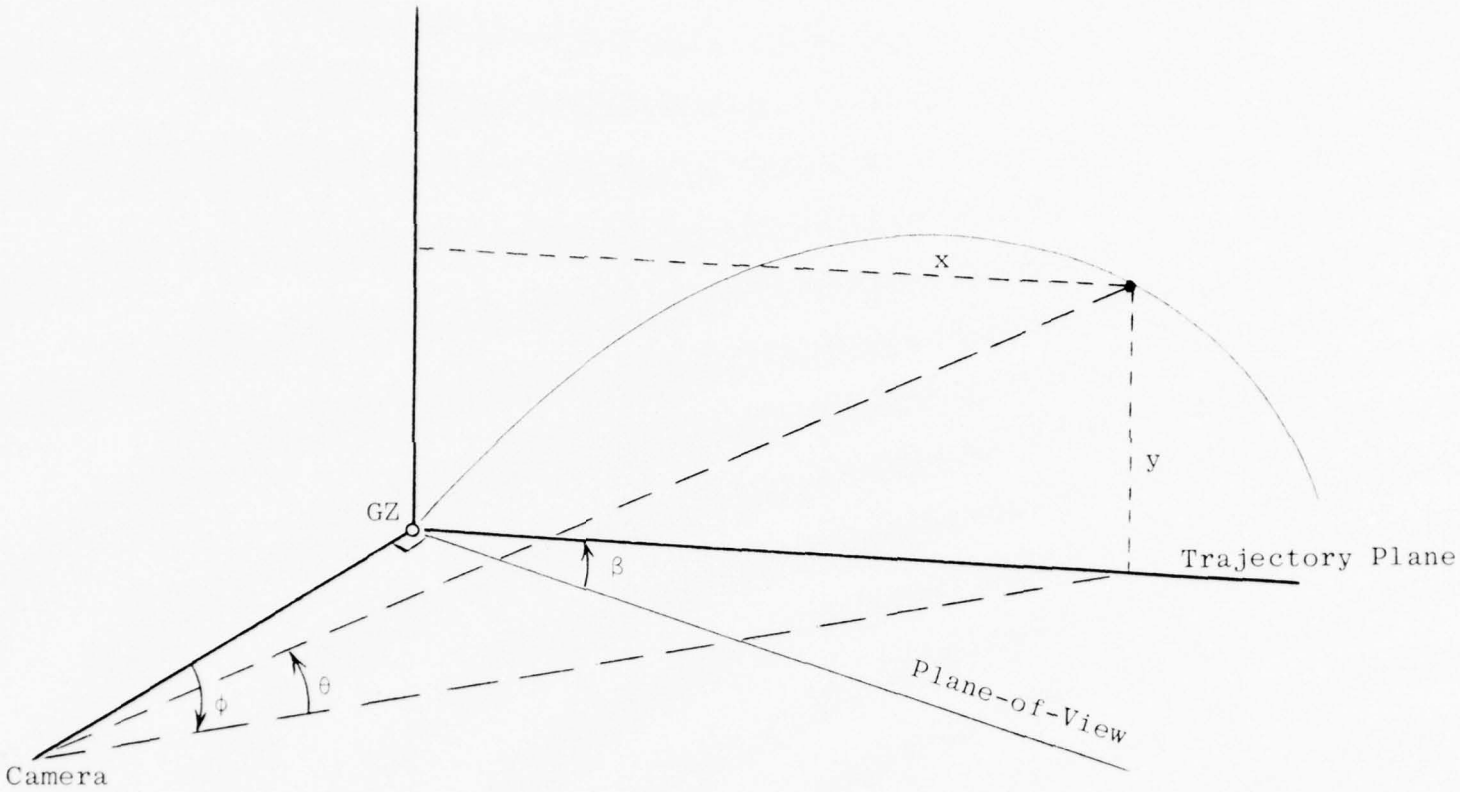

Figure 18 Outline of Camera, GZ and Trajectory Plane

1. Assume an azimuthal ejection angle (β) for the trajectory to be analyzed.

2. Near trajectory peak, use Equation 9 to estimate K by fitting the trajectory points with a second order polynominal.

3. Use this β and K to extrapolate first data points toward origin.

4. If resultant trajectory originates at predetermined location (e.g., final crater radius) assume correct fit in β and K have been found. If not, adjust value for β and repeat above steps.

This approach has several shortcomings which became obvious during an early review of the problem. The derivation of K is biased by an a-priori second order polynominal fit, and the value derived can be dependent on the selected spacing between data points. Most of the acquired digital data is never really used in an optimum fashion and forcing the trajectory toward a preconceived origin also seems faulty. It was felt that the above approach could be improved upon, and that perhaps accurate trajectory data could provide valuable insights to cratering mechanisms and therefore the accuracy and validity of existing cratering models.

An Improved Look at Ejecta Dynamics

Realizing the deficiencies of the above approach, SAI sought to obtain data of improved accuracy and validity by utilizing a direct approach to fit all acquired trajectory data in a least squares test. The approach can be summarized as follows:

Make initial estimates of the dynamic parameters sought (including β), and calculate an ejecta

trajectory through the coupled equations of motion. Compare calculated and experimental trajectory points and minimize, in a least squares sense, the difference between the two sets of information by adjusting the values of the dynamic parameters used in calculating the trajectory.

In concept the above approach is simple. In practice, because of the coupled differential equations of motion (Equations 5 & 6) and because of the trignometric coordinate transformation (Equations 21 & 22), it is considerably more difficult. Development of a detailed computer analysis technique to perform the desired calculations would have been extremely costly and time-consuming, and therefore beyond the scope of the demonstration sought. This rough scoping operation was only made possible by utilizing a proprietary computer language called PROSE, which is a higher order language capable of performing direct calculus calculations (e.g., derivatives are explicitly calculated and carried rather than the digital approximations which are so familiar to most FORTRAN users). Using PROSE, we were able to examine the estimation of ejecta dynamics from the digitized trajectory data, and to make some observations on the validity of the data currently generated.

As mentioned above, the criterion for best estimate in this approach is to minimize the difference between measured and calculated trajectory points. Letting $X(t_i)$, $Y(t_i)$ and $x(t_i)$, $y(t_i)$ be the respective measured and calculated trajectory points at times t_i, we seek to minimize the sum of the N straight line distances between measured and calculated trajectory points:

SUMSQR = Sum of squares =

$$\sum_{i=1}^{N} \left\{ \left| X(t_i) - x(t_i) \right|^2 + \left| Y(t_i) - y(t_i) \right|^2 \right\}^{\frac{1}{2}} \qquad (23)$$

The problem was formulated in PROSE (see Table 2 for typical listing), "ideal" data was generated through the equations of motion and the code was then asked to calculate dynamic parameters from selected portions of the "ideal" data.

For testing purposes, the "ideal" data was limited to two cases; trajectories initiated at a 45^0 elevation angle and a velocity of 200 feet per second, both with and without a drag force. The case with a drag force assumed a "typical" chunk of cohesive dirt with a 30 cm diameter and $C_D \approx 0.6$ so that $K/2 = 9.56 \times 10^{-6}$ (cgs). The trajectories generated for these two cases are shown in Tables 3 and 4. As an approximation to the situation which would be found in the normal analysis procedure, these two trajectories were picked up at three seconds (i.e., just before peak) and data sets of from 10 to 20 points were created. The PROSE-developed code (e.g., Table 2) was then asked to calculate some or all of the dynamic parameters at 3 seconds which could be used as initial conditions to match the "ideal" data through the equations of motion. Note that implicit in this approach is the concept that given the initial conditions at 3 seconds which can be used to duplicate the measured data, then these same conditions can be used to back the trajectory toward the origin to determine ejection parameters. The parameters to be matched in these two cases are listed below in Table 5.

Table 2

Typical PROSE Program Listing for
Ejecta Trajectory Analysis

```
    :L
 10] PROGRAM .GUESS
 20] ALLOT TP(17),XP(17),YP(17),BND(6),AZ(17),EL(17)
 30] READ DATA
 40] SELECT TTY
 50] BND=.DATA(1,1,1,1,1,5)
 60] IMPOSE .SET
 70] FIND F,U0,V0,X0,Y0,BETA IN .TRIP WITH BOUNDS BND TO MINIMIZE SUMSQR
 80] DUMP GLOBALS
 90] END
100] MODEL .TRIP
110] T=TP(1)
120] X=X0
130] Y=Y0
140] U=U0
150] V=V0
160] INITIATE JANISIS FOR .DIFF EQUATIONS
170] UDOT/U, U/X, VDOT/V, V/Y OF T STEP DT
180] SUMSQR=0
190] FOR I=2 TO N  DO
200] UNTIL T GE TP(I)
210] INTEGRATE .DIFF
220] SINAZ=.SIND(AZ(I))
230] COSBP=.COSD(BETA+AZ(I))
240] XP(I)=SINAZ/COSBP
250] YP(I)=.TAND(EL(I))*(1+SINAZ*.SIND(BETA)/COSBP)
260] SUMSQR=SUMSQR+(XP(I)-X)**2+(YP(I)-Y)**2
270] REPEAT
280] END
290] MODEL .DIFF
300] VEL=.SQRT(U*U+V*V)
310] UDOT=-F*U*VEL
320] VDOT=-F*V*VEL-GRAV
330] END
340] CONTROLLER .SET FOR HERA
350] ADJUST=2
355] DELTA=1E-4
360] CONVERGE=1
370] END
   ? :Q
```

Table 3

Case 1 (C_D = 0.6) Ideal Trajectory Used for Data Simulation

time (sec)	dx/dt (cm/sec)	dy/dt (cm/sec)	x (ft)	y (ft)
0.000E-01	4.311E+03	4.311E+03	0.000E-01	0.000E-01
2.500E-01	4.249E+03	4.006E+03	3.511E+01	3.415E+01
5.000E-01	4.192E+03	3.703E+03	6.974E+01	6.533E+01
7.500E-01	4.137E+03	3.416E+03	1.039E+02	9.509E+01
1.000E+00	4.085E+03	3.130E+03	1.376E+02	1.220E+02
1.250E+00	4.036E+03	2.849E+03	1.709E+02	1.465E+02
1.500E+00	3.990E+03	2.572E+03	2.039E+02	1.683E+02
1.750E+00	3.946E+03	2.300E+03	2.364E+02	1.873E+02
2.000E+00	3.904E+03	2.031E+03	2.686E+02	2.036E+02
2.250E+00	3.863E+03	1.767E+03	3.005E+02	2.173E+02
2.500E+00	3.825E+03	1.505E+03	3.320E+02	2.357E+02
2.750E+00	3.788E+03	1.247E+03	3.632E+02	2.470E+02
3.000E+00	3.753E+03	9.903E+02	3.942E+02	2.563E+02
3.250E+00	3.718E+03	7.377E+02	4.248E+02	2.634E+02
3.500E+00	3.685E+03	4.870E+02	4.552E+02	2.684E+02
3.750E+00	3.653E+03	2.387E+02	4.853E+02	2.715E+02
4.000E+00	3.621E+03	-7.496E+00	5.151E+02	2.724E+02
4.250E+00	3.590E+03	-2.515E+02	5.447E+02	2.714E+02
4.500E+00	3.559E+03	-4.935E+02	5.740E+02	2.684E+02
4.750E+00	3.529E+03	-7.334E+02	6.031E+02	2.634E+02
5.000E+00	3.498E+03	-9.712E+02	6.319E+02	2.565E+02
5.250E+00	3.468E+03	-1.207E+03	6.605E+02	2.476E+02
5.500E+00	3.437E+03	-1.440E+03	6.888E+02	2.367E+02
5.750E+00	3.407E+03	-1.671E+03	7.169E+02	2.240E+02
6.000E+00	3.375E+03	-1.900E+03	7.447E+02	2.094E+02
6.250E+00	3.344E+03	-2.127E+03	7.723E+02	1.929E+02
6.500E+00	3.312E+03	-2.350E+03	7.996E+02	1.746E+02
6.750E+00	3.280E+03	-2.571E+03	8.266E+02	1.545E+02
7.000E+00	3.247E+03	-2.789E+03	8.534E+02	1.325E+02
7.250E+00	3.213E+03	-3.004E+03	8.799E+02	1.088E+02
7.500E+00	3.179E+03	-3.216E+03	9.061E+02	8.330E+01

Table 4

Case 2 (No Drag) Ideal Trajectory Used for Data Simulation

time (sec)	dx/dt (cm/sec)	dy/dt (cm/sec)	x (ft)	y (ft)
0.000E-01	4.311E+03	4.311E+03	0.000E-01	0.000E-01
2.500E-01	4.311E+03	4.065E+03	3.536E+01	3.437E+01
5.000E-01	4.311E+03	3.820E+03	7.071E+01	6.673E+01
7.500E-01	4.311E+03	3.575E+03	1.061E+02	9.705E+01
1.000E+00	4.311E+03	3.330E+03	1.414E+02	1.254E+02
1.250E+00	4.311E+03	3.085E+03	1.763E+02	1.517E+02
1.500E+00	4.311E+03	2.840E+03	2.121E+02	1.761E+02
1.750E+00	4.311E+03	2.594E+03	2.475E+02	1.984E+02
2.000E+00	4.311E+03	2.349E+03	2.823E+02	2.187E+02
2.250E+00	4.311E+03	2.104E+03	3.132E+02	2.369E+02
2.500E+00	4.311E+03	1.859E+03	3.536E+02	2.532E+02
2.750E+00	4.311E+03	1.614E+03	3.889E+02	2.675E+02
3.000E+00	4.311E+03	1.369E+03	4.243E+02	2.797E+02
3.250E+00	4.311E+03	1.123E+03	4.596E+02	2.900E+02
3.500E+00	4.311E+03	8.782E+02	4.950E+02	2.982E+02
3.750E+00	4.311E+03	6.330E+02	5.303E+02	3.044E+02
4.000E+00	4.311E+03	3.879E+02	5.657E+02	3.086E+02
4.250E+00	4.311E+03	1.427E+02	6.010E+02	3.108E+02
4.500E+00	4.311E+03	-1.025E+02	6.364E+02	3.110E+02
4.750E+00	4.311E+03	-3.476E+02	6.717E+02	3.092E+02
5.000E+00	4.311E+03	-5.923E+02	7.071E+02	3.053E+02
5.250E+00	4.311E+03	-8.380E+02	7.425E+02	2.995E+02
5.500E+00	4.311E+03	-1.083E+03	7.778E+02	2.916E+02
5.750E+00	4.311E+03	-1.328E+03	8.132E+02	2.815E+02
6.000E+00	4.311E+03	-1.573E+03	8.485E+02	2.693E+02
6.250E+00	4.311E+03	-1.819E+03	8.839E+02	2.550E+02
6.500E+00	4.311E+03	-2.064E+03	9.192E+02	2.401E+02
6.750E+00	4.311E+03	-2.309E+03	9.546E+02	2.222E+02
7.000E+00	4.311E+03	-2.554E+03	9.899E+02	2.022E+02
7.250E+00	4.311E+03	-2.799E+03	1.025E+03	1.803E+02
7.500E+00	4.311E+03	-3.044E+03	1.061E+03	1.564E+02
7.750E+00	4.311E+03	-3.290E+03	1.096E+03	1.304E+02
8.000E+00	4.311E+03	-3.535E+03	1.131E+03	1.024E+02
8.250E+00	4.311E+03	-3.780E+03	1.167E+03	7.247E+01
8.500E+00	4.311E+03	-4.025E+03	1.202E+03	4.045E+01
8.750E+00	4.311E+03	-4.270E+03	1.237E+03	6.475E+00

Table 5

Trajectory parameters at 3 seconds

	Case 1	Case 2
K/2	9.56×10^{-6}	0
x(cm)	12011.3	12932.6
y(cm)	7794.0	8525.3
dx/dt(cm/sec)	3752.7	4311.0
dy/dt(cm/sec)	990.8	1369.0

In all cases the PROSE program is given an initial estimate of the parameter sought and it then iterates through the equations of motion until the desired testing criterion is satisfied; in this case to minimize SUMSQR in Equation 23. As a first test, the analysis routine was asked to calculate the drag force in Case 1 when all other parameters were defined exactly (we ignore β initially). Table 6 is a listing of the 8 iterations on the drag force (called F) which were needed to minimize SUMSQR with an initial guess of 9.6×10^{-6} for F and a 10 data point set. Convergence is fairly rapid (only 25 seconds of total running time on a remote teletype terminal), the calculated drag force is almost exact, and the SUMSQR (or error) is also small. Note if one assumes in SUMSQR that $\Delta X \approx \Delta Y$, then

$$\text{SUMSQR} \approx \sum_{i=1}^{N} 2\Delta X \approx 2N\Delta X \qquad (24)$$

and

$$\Delta X \approx \frac{\text{SUMSQR}}{2N} \quad . \qquad (25)$$

Table 6

Case 1 PROSE Results for Drag Force Only

CONVERGENCE CONDITION AFTER 8 ITERATIONS
UNKNOWNS CONVERGED
OBJECTIVE CRITERION SATISFIED
ALL SPECIFIED CRITERIA SATISFIED

LOOP NUMBER	[INITIAL]	1	2
UNKNOWNS			
F	9.600000E-05	7.600000E-05	5.600000E-05
OBJECTIVE			
SUMSQR	5.889673E+07	4.158849E+07	2.432573E+07

LOOP NUMBER	[INITIAL]	3	4
UNKNOWNS			
F	9.600000E-05	3.600000E-05	1.600000E-05
OBJECTIVE			
SUMSQR	5.889673E+07	1.011935E+07	7.857706E+05

LOOP NUMBER	[INITIAL]	5	6
UNKNOWNS			
F	9.600000E-05	8.508169E-06	9.539754E-06
OBJECTIVE			
SUMSQR	5.889673E+07	2.508311E+04	1.334830E+03

LOOP NUMBER	[INITIAL]	7	8
UNKNOWNS			
F	9.600000E-05	9.565737E-06	9.565753E-06
OBJECTIVE			
SUMSQR	5.889673E+07	1.320702E+03	1.320702E+03

Here SUMSQR is 1320.7, and with N = 10, this implies that $\Delta X \approx 60$ cm over a portion of the trajectory which extends from 12000 cm to 26000 cm.

The PROSE routine was further exercised by asking it next to calculate initial velocity components and then to add initial position coordinates. These results are shown in Tables 7 and 8 and it can be seen that although the number of variables to be determined increased from 1 to 3 and 5, the number of iterations required only went from 8 to 10 and 12. Note also that in the latter case, all five variables have been calculated with errors which are considerably less than one percent. Note also in this case that SUMSQR is only 4.45 or that the average error between the two trajectory coordinates is only 0.2 cm over the same 12000 to 26000 cm range! Similar results and accuracies were obtained for Case 2 (zero drag) as is shown in Table 9, and to test the effects of the initial estimates the 5 parameter Case 1 exercise was rerun with crude initial estimates as shown in Table 10. In the latter case, convergence was accomplished in only 9 iterations, again with accuracies better than one percent.

Having confirmed the validity of this technique with the above tests, trignometric conversions to include the azimuthal ejection angle, β, were included in the PROSE coding and most of the above tests were redone for $\beta = 0$ to assure that no programming errors had been introduced. A new "ideal" data set was then generated for $\beta = 15^0$ using the two cases found in Table 5, and all subsequent testing seemed to indicate that extension to the sixth variable could be accomplished, and that similar accuracies could be anticipated.

However, it soon became apparent that there is a subtle trade-off between azimuthal ejection angle and

Table 7

Case 1 PROSE Results for Drag and Velocity

```
  CONVERGENCE CONDITION AFTER 10 ITERATIONS
     UNKNOWNS CONVERGED
     OBJECTIVE CRITERION SATISFIED
     ALL SPECIFIED CRITERIA SATISFIED

LOOP NUMBER .........    [INITIAL]          1              2
UNKNOWNS
          F            9.600000E-05 -2.307257E-05 -2.875189E-05
         U0            3.720000E+03  4.471570E+03  3.462240E+03
         V0            7.380000E+02  9.740358E+02  1.006497E+03
OBJECTIVE
     SUMSQR            6.222435E+07  1.931211E+03  2.537543E+07

LOOP NUMBER .........    [INITIAL]          3              4
UNKNOWNS
          F            9.600000E-05 -5.090562E-05 -2.841400E-05
         U0            3.720000E+03  2.481274E+03  2.910953E+03
         V0            7.380000E+02  1.065956E+03  1.030666E+03
OBJECTIVE
     SUMSQR            6.222435E+07  1.022423E+07  3.297717E+06

LOOP NUMBER .........    [INITIAL]          5              6
UNKNOWNS
          F            9.600000E-05 -7.571974E-06  4.074229E-06
         U0            3.720000E+03  3.332301E+03  3.611733E+03
         V0            7.380000E+02  1.005092E+03  9.973143E+02
OBJECTIVE
     SUMSQR            6.222435E+07  7.032535E+05  7.062510E+04

LOOP NUMBER .........    [INITIAL]          7              8
UNKNOWNS
          F            9.600000E-05  8.808562E-06  9.514535E-06
         U0            3.720000E+03  3.732973E+03  3.751897E+03
         V0            7.380000E+02  9.955093E+02  9.953774E+02
OBJECTIVE
     SUMSQR            6.222435E+07  1.355361E+03  1.674630E+01

LOOP NUMBER .........    [INITIAL]          9             10
UNKNOWNS
          F            9.600000E-05  9.530563E-06  9.530577E-06
         U0            3.720000E+03  3.752331E+03  3.752331E+03
         V0            7.380000E+02  9.953753E+02  9.953753E+02
OBJECTIVE
     SUMSQR            6.222435E+07  1.606396E+01  1.606396E+01
```

Table 8

Case 1 PROSE Results for Drag, Velocity and Position

LOOP NUMBER	[INITIAL]	1	2	7	8
UNKNOWNS					
F	9.600000E-05	-6.517107E-05	-8.179857E-05	-3.970736E-06	-3.708734E-06
U0	3.718000E+03	3.745950E+03	2.763519E+03	3.243239E+03	3.365166E+03
V0	7.380000E+02	9.099842E+02	1.018948E+03	1.012780E+03	1.027199E+03
X0	1.201500E+04	1.259433E+04	1.134363E+04	1.241873E+04	1.233743E+04
Y0	7.812000E+03	8.032672E+03	8.639231E+03	7.782726E+03	7.746311E+03
OBJECTIVE					
SUMSQR	6.232661E+07	4.578719E+09	3.613639E+08	5.520341E+05	8.691999E+04

LOOP NUMBER	[INITIAL]	3	4	9	10
UNKNOWNS					
F	9.600000E-05	-1.115729E-04	-7.497348E-05	9.253680E-06	8.997666E-06
U0	3.718000E+03	1.775973E+03	2.170511E+03	3.715197E+03	3.736129E+03
V0	7.380000E+02	1.169855E+03	9.711660E+02	9.967997E+02	9.975636E+02
X0	1.201500E+04	1.023102E+04	1.151756E+04	1.202387E+04	1.202704E+04
Y0	7.812000E+03	7.865203E+03	8.502314E+03	7.810237E+03	7.826999E+03
OBJECTIVE					
SUMSQR	6.232661E+07	1.043140E+08	3.194782E+07	2.739653E+04	1.377644E+02

LOOP NUMBER	[INITIAL]	5	6	11	12
UNKNOWNS					
F	9.600000E-05	-5.218005E-05	-3.217939E-05	9.516523E-06	9.514951E-06
U0	3.718000E+03	2.456426E+03	2.686939E+03	3.752032E+03	3.752026E+03
V0	7.380000E+02	1.073324E+03	1.060062E+03	9.963779E+02	9.963823E+02
X0	1.201500E+04	1.254333E+04	1.301343E+04	1.201484E+04	1.201488E+04
Y0	7.812000E+03	7.666510E+03	7.679699E+03	7.809359E+03	7.809347E+03
OBJECTIVE					
SUMSQR	6.232661E+07	4.455693E+06	9.101939E+05	4.533746E+00	4.452411E+00

Table 9

Case 2 PROSE Results for Drag, Velocity and Position

```
  CONVERGENCE CONDITION AFTER  8 ITERATIONS
     UNKNOWNS CONVERGED
     OBJECTIVE CRITERION SATISFIED
     ALL SPECIFIED CRITERIA SATISFIED

LOOP NUMBER .........    [INITIAL]          1              2
UNKNOWNS
          F             9.600000E-06 -2.043821E-05  1.161126E-05
         U0             4.310000E+03  4.116386E+03  5.099665E+03
         V0             1.128000E+03  1.663852E+03  1.617476E+03
         X0             1.293300E+04  1.232144E+04  1.205736E+04
         Y0             3.525000E+03  7.906653E+03  8.147620E+03
OBJECTIVE
     SUMSQR             6.823163E+06  1.126342E+07  1.023273E+06

LOOP NUMBER .........    [INITIAL]          3              4
UNKNOWNS
          F             9.600000E-06  2.055125E-06  1.035704E-06
         U0             4.310000E+03  4.203700E+03  4.357340E+03
         V0             1.128000E+03  1.322472E+03  1.373604E+03
         X0             1.293300E+04  1.263304E+04  1.253337E+04
         Y0             3.525000E+03  3.583967E+03  3.525367E+03
OBJECTIVE
     SUMSQR             6.823163E+06  2.592174E+05  1.276462E+03

LOOP NUMBER .........    [INITIAL]          5              6
UNKNOWNS
          F             9.600000E-06 -4.398266E-08 -2.565521E-08
         U0             4.310000E+03  4.307358E+03  4.308620E+03
         V0             1.128000E+03  1.370743E+03  1.370842E+03
         X0             1.293300E+04  1.293471E+04  1.293381E+04
         Y0             3.525000E+03  3.525900E+03  3.525840E+03
OBJECTIVE
     SUMSQR             6.823163E+06  1.273600E+01  4.317392E+00

LOOP NUMBER .........    [INITIAL]          7              8
UNKNOWNS
          F             9.600000E-06 -2.531066E-08 -2.531066E-08
         U0             4.310000E+03  4.308636E+03  4.308636E+03
         V0             1.128000E+03  1.370842E+03  1.370842E+03
         X0             1.293300E+04  1.293379E+04  1.293379E+04
         Y0             3.525000E+03  3.525841E+03  3.525841E+03
OBJECTIVE
     SUMSQR             6.823163E+06  4.317265E+00  4.317265E+00
```

Table 10

Case 1 PROSE Results with Crude Initial Estimates

LOOP NUMBER	[INITIAL]	1	2
UNKNOWNS			
F	9.600000E-06	5.694695E-06	-2.653203E-05
U0	4.000000E+03	3.763930E+03	3.157043E+03
V0	4.000000E+03	2.640396E+03	1.287792E+03
X0	1.000000E+04	1.033596E+04	1.156500E+04
Y0	1.000000E+04	8.737737E+03	7.695414E+03
OBJECTIVE			
SUMSQR	6.307739E+03	2.005557E+03	7.909403E+06

LOOP NUMBER	[INITIAL]	3	4
UNKNOWNS			
F	9.600000E-06	2.261188E-05	1.494391E-05
U0	4.000000E+03	4.132301E+03	3.970396E+03
V0	4.000000E+03	1.302377E+03	9.554631E+02
X0	1.000000E+04	1.136361E+04	1.178563E+04
Y0	1.000000E+04	7.152823E+03	7.355969E+03
OBJECTIVE			
SUMSQR	6.307739E+03	1.892932E+06	3.572209E+04

LOOP NUMBER	[INITIAL]	5	6
UNKNOWNS			
F	9.600000E-06	3.200870E-06	3.990142E-06
U0	4.000000E+03	3.693882E+03	3.734624E+03
V0	4.000000E+03	1.021849E+03	9.948311E+02
X0	1.000000E+04	1.205554E+04	1.202610E+04
Y0	1.000000E+04	7.737462E+03	7.799305E+03
OBJECTIVE			
SUMSQR	6.307739E+03	3.110783E+03	1.444590E+02

LOOP NUMBER	[INITIAL]	7	8
UNKNOWNS			
F	9.600000E-06	9.494210E-06	9.500636E-06
U0	4.000000E+03	3.751396E+03	3.751671E+03
V0	4.000000E+03	9.935861E+02	9.935695E+02
X0	1.000000E+04	1.201212E+04	1.201191E+04
Y0	1.000000E+04	7.801834E+03	7.801864E+03
OBJECTIVE			
SUMSQR	6.307739E+03	6.184423E+00	6.046310E+00

LOOP NUMBER	[INITIAL]	9
UNKNOWNS		
F	9.600000E-06	9.500700E-06
U0	4.000000E+03	3.751671E+03
V0	4.000000E+03	9.935694E+02
X0	1.000000E+04	1.201191E+04
Y0	1.000000E+04	7.801864E+03
OBJECTIVE		
SUMSQR	6.307739E+03	6.046310E+00

drag force which makes it difficult to resolve the "correct" answer. This trade-off does not appear to be continuous, but has an apparent double value as is typified by the results of Table 11. The PROSE coding in this example could not optimally minimize SUMSQR, but appeared to oscillate around the correct answers calculating drag forces of 1×10^{-5} and 7.6×10^{-6} and azimuthal ejection angles of 14 and 18.6^{0}. This situation is graphically demonstrated in Figure 19 where SUMSQR is plotted as a function of iteration number and the calculated drag and azimuth are also indicated. The coding is obviously not converging on a single answer, and it does not appear that the situation will improve even if the iteration process is allowed to proceed further. (PROSE will automatically terminate the calculational process if an answer has not been obtained after 20 iterations. It can be overridden.) Note also that there is a definite trade-off in drag force and angle as even the relative minimums for SUMSQR are half 14^{0} and 18.6^{0}. There are indications that by appropriately bounding the size of the steps which the code may take in selected variables, that this behavior may be minimized and perhaps even eliminated, but because of time constraints we have not been able to verify this.

It might appear at this point that the goal of obtaining the desired ejection parameters from the trajectory data is unobtainable. However, consider the last two iterations of Table 11 and compare those results with the initial conditions from Table 5. (See Table 12.) Note here that in iteration 19 the calculated parameters of position and velocity differ from the known values by a maximum of 3 percent, while on iteration 20 the difference is less than one percent. What then does this imply with respect to the dynamic parameters at the origin?

Table 11

Case 1 PROSE Result with $\beta = 15^0$, Showing Observed Drag/Angle Ambiguity

LOOP NUMBER	[INITIAL]	1	2
UNKNOWNS			
F	5.000000E-06	-2.460579E-05	-1.130876E-05
U0	4.000000E+03	2.762553E+03	2.846516E+03
V0	8.000000E+02	1.058775E+03	1.049717E+03
X0	1.100000E+04	1.079421E+04	1.094273E+04
Y0	7.000000E+03	7.644679E+03	7.423852E+03
BETA	0.	4.994336E+00	4.510868E+00
OBJECTIVE			
SUMSQR	5.197547E+07	1.923537E+07	6.583671E+05

LOOP NUMBER	[INITIAL]	3	4
UNKNOWNS			
F	5.000000E-06	3.652638E-06	9.916464E-06
U0	4.000000E+03	3.159437E+03	3.332771E+03
V0	8.000000E+02	1.003972E+03	9.894352E+02
X0	1.100000E+04	1.159397E+04	1.145345E+04
Y0	7.000000E+03	7.520015E+03	7.541225E+03
BETA	0.	3.690604E+00	3.456256E+00
OBJECTIVE			
SUMSQR	5.197547E+07	1.934119E+05	3.379671E+04

LOOP NUMBER	[INITIAL]	5	6
UNKNOWNS			
F	5.000000E-06	1.453595E-05	1.232530E-05
U0	4.000000E+03	3.461253E+03	3.561326E+03
V0	8.000000E+02	9.805950E+02	9.833614E+02
X0	1.100000E+04	1.136313E+04	1.152557E+04
Y0	7.000000E+03	7.562362E+03	7.659227E+03
BETA	0.	3.637910E+00	3.575044E+00
OBJECTIVE			
SUMSQR	5.19 547E+07	9.723369E+03	9.715005E+04

LOOP NUMBER	[INITIAL]	7	8
UNKNOWNS			
F	5.000000E-06	1.265769E-05	1.066536E-05
U0	4.000000E+03	3.576294E+03	3.693883E+03
V0	.000000E+02	9.840843E+02	9.830201E+02
X0	1.100000E+04	1.157557E+04	1.183341E+04
Y0	7.000000E+03	7.661653E+03	7.758903E+03
BETA	0.	3.644046E+00	1.341334E+01
OBJECTIVE			
SUMSQR	5.197547E+07	3.435235E+03	1.093502E+05

LOOP NUMBER	[INITIAL]	9	10
UNKNOWNS			
F	5.000000E-06	1.028636E-05	8.256900E-06
U0	4.000000E+03	3.703534E+03	3.847636E+03
V0	8.000000E+02	9.892233E+02	9.936600E+02
X0	1.100000E+04	1.139839E+04	1.223773E+04
Y0	7.000000E+03	7.761571E+03	7.862601E+03
BETA	0.	1.347165E+01	1.807804E+01
OBJECTIVE			
SUMSQR	5.197547E+07	1.217893E+03	1.289414E+05

Table 11 (Continued)

LOOP NUMBER	[INITIAL]	11	12
UNKNOWNS			
F	5.000000E-06	7.897114E-06	1.032340E-05
U0	4.000000E+03	3.857735E+03	3.693533E+03
V0	8.000000E+02	9.947308E+02	9.355953E+02
X0	1.100000E+04	1.229823E+04	1.135862E+04
Y0	7.000000E+03	7.363544E+03	7.764247E+03
BETA	0.	1.811512E+01	1.372489E+01
OBJECTIVE			
SUMSQR	5.197547E+07	1.539292E+03	1.123323E+05

LOOP NUMBER	[INITIAL]	13	14
UNKNOWNS			
F	5.000000E-06	1.027126E-05	8.110267E-06
U0	4.000000E+03	3.710316E+03	3.853289E+03
V0	8.000000E+02	9.394782E+02	9.940332E+02
X0	1.100000E+04	1.191563E+04	1.226641E+04
Y0	7.000000E+03	7.767696E+03	7.367130E+03
BETA	0.	1.377003E+01	1.836599E+01
OBJECTIVE			
SUMSQR	5.197547E+07	1.193210E+03	1.311247E+05

LOOP NUMBER	[INITIAL]	15	16
UNKNOWNS			
F	5.000000E-06	7.747693E-06	1.016378E-05
U0	4.000000E+03	3.868502E+03	3.787437E+03
V0	8.000000E+02	9.951165E+02	9.839498E+02
X0	1.100000E+04	1.232713E+04	1.138223E+04
Y0	7.000000E+03	7.872295E+03	7.778656E+03
BETA	0.	1.840254E+01	1.402728E+01
OBJECTIVE			
SUMSQR	5.197547E+07	1.655120E+03	1.132235E+05

LOOP NUMBER	[INITIAL]	17	18
UNKNOWNS			
F	5.000000E-06	9.914719E-06	7.963561E-06
U0	4.000000E+03	3.719273E+03	3.869279E+03
V0	8.000000E+02	9.898295E+02	9.944105E+02
X0	1.100000E+04	1.193932E+04	1.229547E+04
Y0	7.000000E+03	7.774113E+03	7.873711E+03
BETA	0.	1.407272E+01	1.865462E+01
OBJECTIVE			
SUMSQR	5.197547E+07	1.146252E+03	1.326939E+05

LOOP NUMBER	[INITIAL]	19	20
UNKNOWNS			
F	5.000000E-06	7.681534E-06	1.000525E-05
U0	4.000000E+03	3.879529E+03	3.716528E+03
V0	8.000000E+02	9.955021E+02	9.893013E+02
X0	1.100000E+04	1.235639E+04	1.190629E+04
Y0	7.000000E+03	7.876696E+03	7.777185E+03
BETA	0.	1.369214E+01	1.433027E+01
OBJECTIVE			
SUMSQR	5.197547E+07	1.730326E+03	1.141039E+05

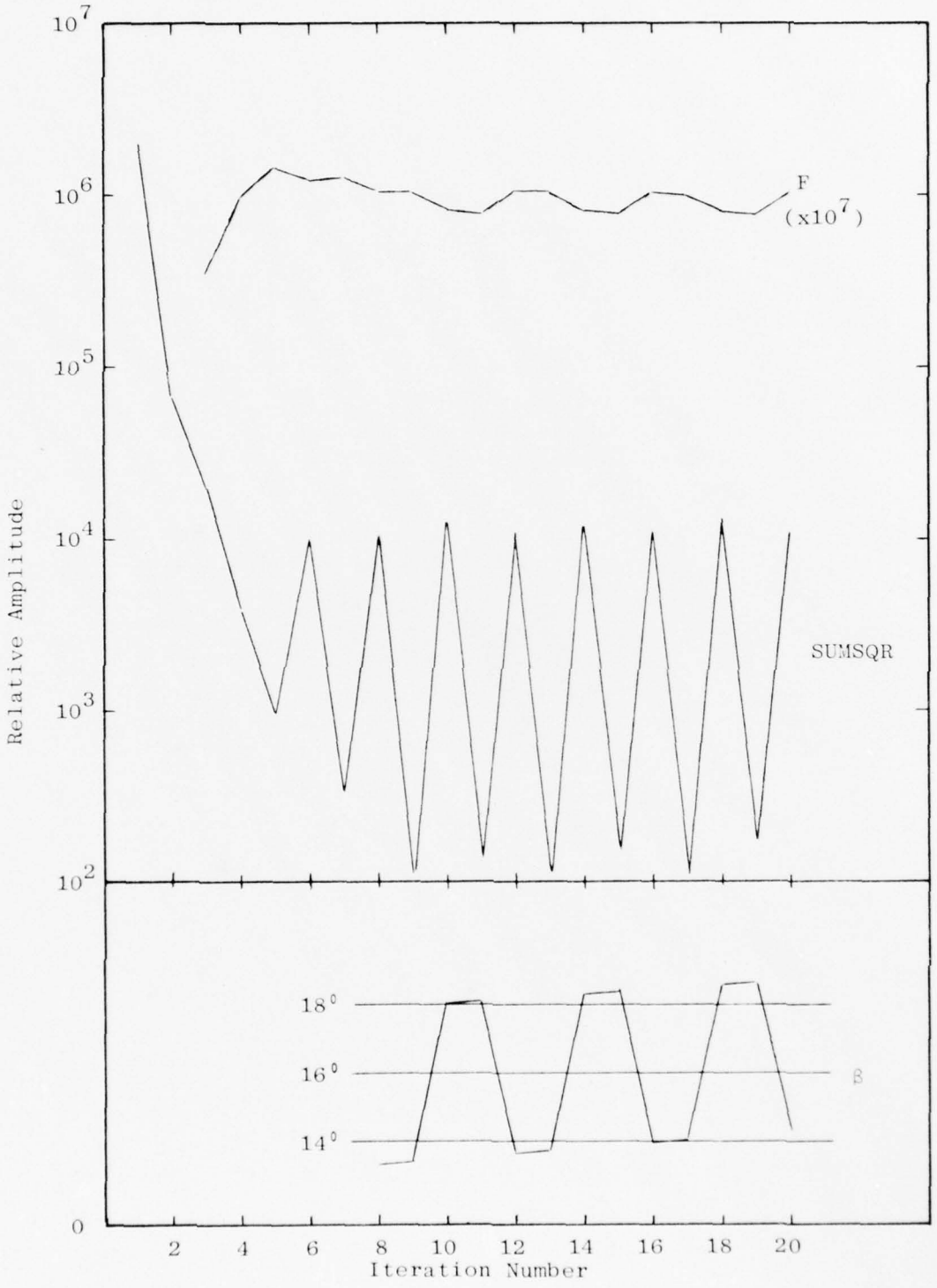

Figure 19 Change in SUMSQR, β and F as a Function of Iteration Number

Table 12

Comparison of Known and Calculated
Dynamic Parameters at 3 Seconds

	Case 1 (Input)	Iteration 19	Iteration 20
F	9.57×10^{-6}	7.60×10^{-6}	1.00×10^{-6}
dx/dt(cm/sec)	3,753	3,879	3,717
dy/dt(cm/sec)	991	996	989
x(cm)	12,011	12,356	11,906
y(cm)	7,794	7,877	7,777
β(degrees)	15	18.7	14.3

The calculated parameters of Table 12 were used as initial conditions in the differential equations of motion and the respective trajectories were traced back toward the origin. These results are again compared below:

Table 13

Comparison of Known and Calculated
Dynamic Parameters at 0.25 Seconds

	Input	Iteration 19	Iteration 20
F	9.57×10^{-6}	7.60×10^{-6}	1.00×10^{-6}
dx/dt(cm/sec)	4249	4288	4229
dy/dt(dm/sec)	4006	3946	4018
x(cm)	1070	1172	1047
y(cm)	1041	1179	1021

We see here that propagating the three percent errors of Table 12 thru the equations of motion result in errors as high as thirteen percent, but more generally of only several percent. The larger positional errors of iteration 19 would place the ejecta at 38 feet in x,y as opposed to the correct 34 to 35 feet, but then again this is probably better accuracy than one could hope to obtain from any cratering calculation (note that velocity errors, for either iteration, are definitely less than two percent).

Although we have not definitively demonstrated the feasibility of obtaining ejecta dynamic parameters with sufficient accuracy to correlate with cratering calculations, the above demonstration would seem to imply that the suggested technique has sufficient merit to warrant further examination. The simplicity of concept and the lack of preconceived bounds or constraints on allowable solutions should also prove appealing. In essence, this approach is straightforward curve fitting (calculated versus measured trajectories) which utilizes all of the acquired data to generate a solution to a non-linear optimal estimation problem. Note also that in the generation of SUMSQR we automatically obtain a measure of the goodness of fit between measured and calculated trajectories.

V. CONCLUSIONS AND RECOMMENDATIONS

The work reviewed in this report has considered in-flight sizing for ejecta from the MIDDLE GUST high explosive test series, and has also examined in some detail the feasibility of obtaining initial dynamic ejecta characteristics for correlation with cratering calculations. Both efforts have made significant contributions to our understanding of the cratering process and of ejecta dynamics. Each is considered more fully below.

In-Flight Sizing

The ejecta sizing measurements presented in Section III tend to support the $a^{-3.5}$ or $a^{-4.0}$ power law currently employed in the SAI ejecta model. As noted in this report, these distributions (and hence this conclusion) hold most specifically for the farther-out or discontinuous ejecta blanket as close-in measurements could not be made because of the dust/combustion products cloud. The support which these measurements provide only becomes apparent after detailed comparison with ejecta fields predicted by the SAI model. Gravitational and aerodynamic filtering of the initial size distributions create the fields which can be used for direct comparisons such as that shown in Figure 4.

Although calibration shot 9, over a shale geology, tended to produce more ejecta than the other calibration shots, the general shape of the distributions was similar. The calibration shots and the 20 ton shot

were all half-buried and therefore the data presented for them are directly comparable as there is no variation in shot geometry. For these shots an increase in yield by a factor of 40 (0.5 to 20 ton) increases ejecta yield by a factor of 10 to 20.

If there is sufficient interest in the impact characteristics of the discontinuous ejecta field, these measurements should be pursued to cover other geologies and shot configurations. At best, the data acquired to date does not contradict the existing ejecta size model, but not enough data has been acquired to perform a definitive validation.

Ejecta Dynamics

Although existing analysis techniques may provide data on ejecta dynamics which is of sufficient accuracy for certain applications, a better knowledge of ejecta trajectories may provide data of sufficient accuracy and validity to permit direct comparison with (and hopefully validation of) existing cratering models. The approach reviewed here has such promise and does not rely upon preconceived bounds or constraints to permit identification of the "correct" solution.

This problem has been approached with a unique and powerful programming tool (PROSE) which made the entire investigation feasible within the existing constraints. Although this investigation has revealed an inherent ambiguity between the drag force and the azimuthal ejection angle, it is an ambiguity which is not unique to this approach. Other analysis techniques have the same ambiguity, but have not been able to recognize it because of their coarseness.

It is felt that the approach suggested here has sufficient merit to warrant further investigation,

particularly with respect to developing tools which will permit resolving this ambiguity. There are constraints available, within the PROSE system, on exactly how certain variables may be approached and/or approximated (not on their final value) and these may offer a simple solution to the problem. With the development of a validated analysis technique, DNA must then decide whether or not a correlation of ejecta dynamics and cratering models merits further work.

REFERENCES

1. Seebaugh, W.R., "A Dynamic Crater Ejecta Model," Science Applications, Inc., SAI-76-654-WA, In Press, October 1976.

2. Layson, W.M., et al. Private Communication, General Research Corporation, August 1969.

3. Gault, D.E., Shoemaker, E.M., and Moore, H.T., "Spray Ejected from the Lunar Surface by Meteoroid Impact," NASA TND-1767, April 1963.

4. Linnerud, J.J., "In-Flight Ejecta Size Distributions for MIDDLE GUST III," Science Applications, Inc., SAI-74-502-BN, DNA3574F, March 1975.

5. Seebaugh, W.R., "Studies of the Nuclear Crater Ejecta Environment," Science Applications, Inc., SAI-75-507-WA, DNA3604F, June 1975.

6. Wisotski, J., "MIDDLE GUST Dynamic Ejecta Measurements," Denver Research Institute, In Press, July 1974.

7. Linnerud, H.J., "Ejecta Sizing for MIDDLE GUST III -- A Feasibility Demonstration," Science Applications, Inc., SAI-73-503-BN, July 1973.

8. Linnerud, H. J., "MIDDLE GUST I Ejecta Sizing and an Examination of Ejecta Ballistics," Science Applications Inc., SAI-76-504-BO, DNA Final Report, In Press, February 1976.

9. Wisotski, J., "MIDDLE NORTH Series, MIXED COMPANY Events," Denver Research Institute, DRI2659, POR6625, August 1975.

APPENDIX

TABULATED SIZING DATA FOR MG CALIBRATION EVENTS

TABLE 1

INTEGRAL EJECTA COUNT FOR CALIBRATION SHOT 3a

Area		2 sec	4 sec
pp^2	cm^2	West	West
10	1.3	3722	6131
20	2.6	3271	5030
40	5.3	2787	3781
60	7.9	2477	3024
80	10.6	2237	2473
100	13.2	2022	2088
200	26.4	1378	1149
300	39.6	1011	774
400	52.8	780	549
800	105.6	370	216
1000	132.0	301	151
2000	263.9	104	36

TABLE 2

INTEGRAL EJECTA COUNT FOR CALIBRATION SHOT 6

Area		2 sec	2 sec	4 sec	6 sec
pp^2	cm^2	West	East	West	West
10	2.9	3331	2220	2477	1972
20	5.9	2763	1847	1961	1406
40	11.8	2205	1492	1376	921
60	17.8	1838	1277	1054	668
80	23.7	1563	1134	827	473
100	29.6	1329	1005	662	338
200	59.3	662	599	261	108
300	88.9	420	430	132	43
400	118.6	293	305	71	24
800	237.3	103	132	16	--
1000	296.6	80	96	8	--
2000	593.2	19	28	2	--

TABLE 3

INTEGRAL EJECTA COUNT FOR CALIBRATION SHOT 8

Area		2 sec West	2 sec East	4 sec West	6 sec West
pp^2	cm^2				
10	3.7	1751	2002	2528	2776
20	7.5	1503	1668	2146	2196
40	15.0	1319	1343	1764	1498
60	22.5	1202	1137	1517	1172
80	30.0	1101	995	1339	952
100	37.6	1021	869	1182	817
200	75.1	711	523	692	434
300	112.6	550	348	482	269
400	150.2	460	253	333	197
800	300.4	247	94	109	58
1000	375.5	190	69	56	40
2000	751.0	88	19	8	2

TABLE 4

INTEGRAL EJECTA COUNT FOR CALIBRATION SHOT 9

Area		2 sec	2 sec	4 sec	6 sec
pp^2	cm^2	West	East	West	West
10	3.8	6612	6506	5209	3025
20	7.6	4973	5196	3996	1915
40	15.1	3659	3969	2941	1218
60	22.7	3012	3215	2408	885
80	30.3	2534	2682	2044	683
100	37.9	2218	2299	1764	533
200	75.7	1310	1283	983	220
300	113.6	894	802	570	124
400	151.4	640	569	375	79
800	302.9	274	194	89	22
1000	378.6	175	145	49	12
2000	757.2	38	32	1	3

DISTRIBUTION LIST

DEPARTMENT OF DEFENSE

Director
Defense Advanced Research Proj. Agency
ATTN: NMRO
ATTN: PMO
ATTN: STO
ATTN: Technical Library

Director
Defense Civil Preparedness Agency
Assistant Director for Research
ATTN: Admin. Officer

Defense Communications Agency
WWMCCS System Engineering Org.
ATTN: Thomas Neighbors

Defense Documentation Center
12 cy ATTN: TC

Director
Defense Intelligence Agency
ATTN: DT-1C
ATTN: DI-7E
ATTN: DB-4C, Edward O'Farrell

Director
Defense Nuclear Agency
3 cy ATTN: STTL, Tech. Library
ATTN: DDST
2 cy ATTN: SPSS
ATTN: STSI, Archives

Dir. of Defense Research & Engineering
Department of Defense
ATTN: S&SS (OS)
ATTN: AD/SW
ATTN: DD/TWP

Commander
Field Command
Defense Nuclear Agency
ATTN: FCPR

Director
Interservice Nuclear Weapons School
ATTN: Document Control

Director
Joint Strat. Target Planning Staff, JCS
ATTN: STINFO Library

Chief
Livermore Division, Field Command, DNA
Lawrence Livermore Laboratory
ATTN: FCPRL

DEPARTMENT OF THE ARMY

Director
BMD Advanced Tech. Center
Huntsville Office
ATTN: CRDABH-S
ATTN: 1CRDABH-X

DEPARTMENT OF THE ARMY (Continued)

Dep. Chief of Staff for Research Dev. & Acq.
Department of the Army
ATTN: Technical Library

Chief of Engineers
Department of the Army
ATTN: DAEN-MCE-D
ATTN: DAEN-RDM

Deputy Chief of Staff for Ops. & Plans
Department of the Army
ATTN: Technical Library

Commander
Harry Diamond Laboratories
ATTN: DRXDO-NP
ATTN: DRXDO-TI, Tech. Lib.

Commander
Redstone Scientific Information Center
US Army Missile Command
ATTN: Chief, Documents

Director
US Army Ballistic Research Labs.
ATTN: DRXBR-X, Julius J. Meszaros
ATTN: DRXBR-TL-1R, J. H. Keefer
ATTN: W. Taylor
ATTN: Tech. Lib., Edward Baicy

Commander
US Army Engineer Center
ATTN: ATSEN-SY-L

Division Engineer
US Army Engineer Div. Huntsville
ATTN: HNDED-SR

Division Engineer
US Army Engineer Div. Ohio River
ATTN: Technical Library

Director
US Army Engr. Waterways Exper. Sta.
ATTN: Guy Jackson
ATTN: John N. Strage
ATTN: Leo Ingram
ATTN: William Flathau
ATTN: Technical Library

Commander
US Army Mat. & Mechanics Research Center
ATTN: Technical Library

Commander
US Army Materiel Dev. & Readiness Command
ATTN: Technical Library

Commander
US Army Nuclear Agency
ATTN: Tech. Lib.

DEPARTMENT OF THE NAVY

Chief of Naval Material
Navy Department
ATTN: MAT 0323

Chief of Naval Operations
Navy Department
ATTN: OP 981
ATTN: OP 03EG

Chief of Naval Research
Navy Department
ATTN: Nicholas Perrone
ATTN: Jacob L. Warner, Code 464
ATTN: Technical Library
ATTN: Thomas P. Quinn, Code 464

Officer-In-Charge
Civil Engineering Laboratory
Naval Construction Battalion Cen.
ATTN: Stan Takahashi
ATTN: Technical Library

Commander
David W. Taylor Naval Ship R & D Center
ATTN: Code L42-3, Library

Commander
Naval Electronic Systems Command
Naval Electronic Systems Command Headquarters
ATTN: PME 117-21A

Commander
Naval Facilities Engineering Command
Headquarters
ATTN: Code 03A
ATTN: Technical Library
ATTN: Code 04B

Superintendent (Code 1424)
Naval Postgraduate School
ATTN: Code 2124, Tech. Rpts. Librarian

Director
Naval Research Laboratory
ATTN: Code 2600, Tech. Lib.

Commander
Naval Sea Systems Command
Navy Department
ATTN: ORD-91313, Lib.

Commander
Naval Ship Engineering Center
Department of the Navy
ATTN: Technical Library

Commander
Naval Ship Research and Development Center
Underwater Explosive Research Division
ATTN: Technical Library

Commander
Naval Surface Weapons Center
ATTN: Code WA501, Navy Nuc. Prgms. Off.

Commander
Naval Surface Weapons Center
Dahlgren Laboratory
ATTN: Technical Library

DEPARTMENT OF THE NAVY (Continued)

President
Naval War College
ATTN: Technical Library

Commanding Officer
Naval Weapons Evaluation Facility
ATTN: Technical Library

Director
Strategic Systems Project Office
Navy Department
ATTN: NSP-43, Tech. Lib.

DEPARTMENT OF THE AIR FORCE

AF Geophysics Laboratory, AFSC
ATTN: SUOL, Research Lib.

AF Institute of Technology, AU
ATTN: Library AFIT, Bldg. 640, Area B

AF Weapons Laboratory, AFSC
ATTN: SUL
ATTN: DEP, Jimmie L. Bratton
ATTN: DES-S, M. A. Plamondon
ATTN: DYT
ATTN: DES-C, Robert Henny

Headquarters
Air Force Systems Command
ATTN: DLCAW
ATTN: Technical Library

Commander
Foreign Technology Division, AFSC
ATTN: NICD, Library

Hq. USAF/IN
ATTN: INATA

Hq. USAF/PR
ATTN: PRE

Hq. USAF/RD
ATTN: RDQSM

Commander
Rome Air Development Center, AFSC
ATTN: EMTLD, Doc. Library

SAMSO/MN
ATTN: MNH

Commander In Chief
Strategic Air Command
ATTN: NRI-STINFO, Library

ENERGY RESEARCH & DEVELOPMENT ADMINISTRATION

University of California
Lawrence Livermore Laboratory
ATTN: Tech. Info., Dept. L-3

Los Alamos Scientific Laboratory
ATTN: Doc. Con. for R. J. Bridwell
ATTN: Doc. Con. for G. R. Spillman
ATTN: Doc. Con. for Reports Lib.

ENERGY RESEARCH & DEVELOPMENT ADMINISTRATION (Continued)

Sandia Laboratories
Livermore Laboratory
ATTN: Doc. Control for Tech. Library

Sandia Laboratories
ATTN: Doc. Con. for 3141, Sandia Rpt. Coll.

US Energy Research & Development Admin.
Albuquerque Operations Office
ATTN: Doc. Con. for Tech. Library

US Energy Research & Dev. Admin.
Division of Headquarters Services
ATTN: Doc. Con. for Class Tech. Lib.

US Energy Research & Dev. Admin.
Nevada Operations Office
ATTN: Doc. Con. for Tech. Lib.

Union Carbide Corporation
Holifield National Laboratory
ATTN: Doc. Con. for Tech. Lib.
ATTN: Civil Def. Res. Proj.

OTHER GOVERNMENT AGENCIES

Department of the Interior
Bureau of Mines
ATTN: Tech. Lib.

Department of the Interior
US Geological Survey
ATTN: Cecil B. Raleigh
ATTN: J. H. Healy

DEPARTMENT OF DEFENSE CONTRACTORS

Aerospace Corporation
ATTN: Tech. Info. Services

Agbabian Associates
ATTN: M. Agbabian

Applied Theory, Inc.
2 cy ATTN: John G. Trulio

AVCO Research & Systems Group
ATTN: Research Lib., A830, Rm. 7201

Battelle Memorial Institute
ATTN: Technical Library

The BDM Corporation
ATTN: Technical Library

The Boeing Company
ATTN: Aerospace Library
ATTN: R. M. Schmidt

California Research & Technology, Inc.
ATTN: Sheldon Shuster
ATTN: Technical Library
ATTN: Ken Kreyenhagen

Calspan Corporation
ATTN: Technical Library

Civil/Nuclear Systems Corp.
ATTN: Robert Crawford

DEPARTMENT OF DEFENSE CONTRACTORS (Continued)

University of Dayton
Industrial Security Super KL-505
ATTN: Hallock F. Swift

University of Denver
Colorado Seminary
Denver Research Institute
ATTN: Sec. Officer for J. Wisotski

EG&G, Inc.
Albuquerque Division
ATTN: Technical Library

Gard, Incorporated
ATTN: G. L. Neidhardt

General Electric Company
TEMPO-Center for Advanced Studies
ATTN: DASIAC

IIT Research Institute
ATTN: Technical Library

Institute for Defense Analyses
ATTN: IDA Librarian, Ruth S. Smith

Kaman AviDyne
Division of Kaman Sciences Corp.
ATTN: Technical Library
ATTN: E. S. Criscione

Kaman Sciences Corporation
ATTN: Library

Lockheed Missiles & Space Co., Inc.
ATTN: Technical Library

Lockheed Missiles & Space Co., Inc.
ATTN: Tech. Info. Center, D/COLL
ATTN: Tom Geers, D/52-33, Bldg. 205

McDonnell Douglas Corporation
ATTN: Robert W. Halprin

Merritt Cases, Incorporated
ATTN: Technical Library
ATTN: J. L. Merritt

The Mitre Corporation
ATTN: Library

Nathan M. Newmark
Consulting Engineering Services
ATTN: Nathan M. Newmark

Physics International Company
ATTN: Doc. Con. for Charles Godfrey
ATTN: Doc. Con. for Fred M. Sauer
ATTN: Doc. Con. for Robert Swift
ATTN: Doc. Con. for Larry A. Behrmann
ATTN: Doc. Con. for E. T. Moore
ATTN: Doc. Con. for Tech. Lib.
ATTN: Doc. Con. for Dennis Orphal

DEPARTMENT OF DEFENSE CONTRACTORS (Continued)

R & D Associates
ATTN: Technical Library
ATTN: Henry Cooper
ATTN: Jerry Carpenter
ATTN: William B. Wright, Jr.
ATTN: Cyrus P. Knowles
ATTN: Harold L. Brode
ATTN: Robert Port
ATTN: J. G. Lewis
ATTN: Jerry Stockton

Science Applications, Inc.
ATTN: D. E. Maxwell
ATTN: David Berstein

Science Applications, Inc.
ATTN: Harold J. Linnerud

Science Applications, Inc.
ATTN: Technical Library

Southwest Research Institute
ATTN: A. B. Wenzel
ATTN: Wilfred E. Baker

Stanford Research Institute
ATTN: George R. Abrahamson
ATTN: Burt R. Gasten

Systems, Science and Software, Inc.
ATTN: Technical Library
ATTN: Ted Cherry
ATTN: Thomas D. Riney
ATTN: Donald R. Grine

Terra Tek, Inc.
ATTN: Technical Library
ATTN: Sidney Green

DEPARTMENT OF DEFENSE CONTRACTORS (Continued)

Tetra Tech., Inc.
ATTN: Technical Library
ATTN: Li-San Hwang

TRW Systems Group
ATTN: Tech. Info. Center/S-1930
ATTN: R. K. Plebuch, R1-2078
ATTN: I. E. Alber, R1-1008
2 cy ATTN: Peter K. Dai, R1/2170
ATTN: D. H. Baer, R1-2136

TRW Systems Group
San Bernardino Operations
ATTN: E. Y. Wong, 527/712

Universal Analytics, Inc.
ATTN: E. I. Field

URS Research Company
ATTN: Technical Library

The Eric H. Wang, Civil Engineering Rsch. Fac.
The University of New Mexico
ATTN: Larry Bickle
ATTN: Neal Baum

Washington State University
Administrative Office
Arthur Miles Hohorf
ATTN: George Duval

Weidlinger Assoc. Consulting Engineers
ATTN: Melvin L. Baron
ATTN: J. W. Wright

Weidlinger Assoc. Consulting Engineers
ATTN: J. Isenberg

Westinghouse Electric Company
Marine Division
ATTN: W. A. Volz